National Défense
Defence nationale

AN INVESTIGATION OF CFAR TECHNIQUES FOR AIRBORNE RADARS

by

G. Vrckovnik and D. Faubert

DEFENCE RESEARCH ESTABLISHMENT OTTAWA
REPORT NO.1056

Canada

December 1990
Ottawa

National Defence / Défense nationale

AN INVESTIGATION OF CFAR TECHNIQUES FOR AIRBORNE RADARS

by

G. Vrckovnik and D. Faubert
Airborne Radar Section
Radar Division

DEFENCE RESEARCH ESTABLISHMENT OTTAWA
REPORT NO.1056

PCN
021LA

December 1990
Ottawa

ABSTRACT

In this report, techniques for performing constant false alarm rate (CFAR) processing with airborne pulse-Doppler radars are described. Cell-averaging, greatest-of, and smallest-of CFAR processors are implemented on interference environments of thermal noise, and thermal noise plus clutter. For the particular radar conditions considered, a 60 dB clutter peak appears across all of the range gates, and thirty of the Doppler bins. While these three processors were successful in the thermal noise environment, they suffered large CFAR losses in the presence of the clutter peak. The smallest-of CFAR algorithm performed much worse than the other two, due to its tendency to underestimate the interference powers. Although enlarging the reference window improves the performance of all the processors, it is clear that for the complicated clutter situation examined, more sophisticated CFAR techniques are required.

RÉSUMÉ

Ce rapport décrit des techniques pour réaliser des taux constants de fausses alarmes (TCFA) pour des radars aéroportés. La moyenne cellulaire, le plus-grand-de et le plus-petit-de TCFA processeurs sont impiantés pour des situations d'interférence de bruit thermique, et aussi de bruit plus fouillis. Pour les conditions radars particulières considérées dans l'étude, un pic de fouillis de 60 dB apparaît dans toutes les cellules de portée et sur une largeur de 30 cellules Doppler. Bien que les trois processeurs aient une bonne performance dans un environnement de bruit thermique, ils montrent une large perte TCFA en présence du pic de fouillis. À cause de sa tendance à sous-estimer les puissances d'interférence, le plus-petit-de TCFA algorithme a une performance beaucoup plus pauvre que les deux autres algorithmes. Bien qu'un élargissement de la grandeur de la fenêtre de référence améliore la performance des trois processeurs, il est clair que pour le cas compliqué où il y a du fouillis avec des caractéristiques semblables à celles de la situation étudiée, des techniques TCFA plus sophistiquées sont nécessaires.

EXECUTIVE SUMMARY

Constant false alarm rate (CFAR) processors are used to prevent automatic detection radar systems from becoming overloaded with false targets in the presence of time varying, or unknown interference environments. They are also used to maintain the number of false alarms at a level which is consistent with the particular operating scenario. Many different CFAR algorithms exist; among the most common are the cell-averaging, greatest-of, and smallest-of processors. These three processors were implemented and compared in airborne pulse-Doppler radar interference environments of thermal noise, and thermal noise plus clutter. It was found that the smallest-of CFAR algorithm performed poorly because it tends to underestimate the interference power. The cell-averaging and greatest-of processors produced results of comparable quality in both types of interference. Although they were very successful in the thermal noise cases, their performance decreased substantially when faced with the large clutter peak (60 dB) that arose from the conditions considered in this report. More sophisticated techniques will be required to negate the effects produced by this clutter peak.

TABLE OF CONTENTS

LIST OF FIGURES

LIST OF FIGURES CONTINUED

LIST OF TABLES

1.0 INTRODUCTION TO CFAR

Modern radar systems support automatic detection modes in which some function of the envelope detector output at a range-Doppler resolution cell is compared with a threshold number, T. If the threshold is exceeded, then a target is declared to be present. The threshold value is selected to provide the maximum false alarm rate that the radar system signal and data processors can accommodate, without becoming overloaded. Increasing the detection threshold unnecessarily results in desensitization of the radar system to target returns.

The threshold value is a function of the design false alarm probability and the level of the surrounding interference. That is,

$$T = k_0 \sigma_0^2 \tag{1}$$

where σ_0^2 is the ambient interference power and k_0 is a proportionality constant controlling the false alarm rate.

Usually the threshold for this processor assumes a value that is appropriate for a thermal noise environment. However, for practically all realistic operating scenarios, the interference power is made up of thermal noise plus the return echoes from a large number of point, area or extended targets, known as clutter. Unfortunately, the false alarm probability, when operating in an automatic detection mode given by (1), is extremely sensitive to small variations in the interference power. Finn and Johnson [1] demonstrated that for a case in which the threshold was originally set for a false alarm probability of 10^{-8}, a 3 dB increase in the total noise power density (thermal noise and clutter) resulted in a new false alarm probability of 10^{-4}. Since virtually all radar systems operate in environments in which the interference level is time-varying, and possibly unknown a priori, automatic target detection with a fixed threshold scheme is not practical.

Constant false alarm rate (CFAR) processors alleviate the problems of automatic target detection when the interference power is unknown or time varying. The goal of a CFAR processor is to maintain a constant false alarm probability, while maximizing the detection probability. It does so by estimating the interference power in the resolution cell under examination. A target is declared to be present if the power in the cell under test exceeds some fixed multiple of the estimated interference power.

Many different CFAR techniques exist [2-10]. Some make no a priori assumptions about the form of the background noise or clutter distributions. These nonparametric, or distribution-free detectors are intended to provide CFAR operation in the presence of unknown or varying background noise and clutter-envelope statistics [2]. Other CFAR techniques assume that for detection over an observation interval, the interference distribution is completely known except for a finite number of parameters, and that the distribution type is fixed except for possible variation in one or more of the distribution parameters.

The work described in this report makes use of the latter of the CFAR techniques. That is, the interference power distribution in the cell under test is assumed to be known, except for the mean power μ_i. Thus if X_i is the squared modulus of the interference in cell i, its cumulative distribution, $F_{X_i}(x)$, is given by

$$F_{X_i}(x) = P(X_i < x) = F_u\left(\frac{x}{\mu_i}\right) \tag{2}$$

where $F_u(x)$ is the unit mean distribution.

The distribution type used in this report is the exponential distribution. An exponential power distribution corresponds to an interference environment having a Rayleigh-envelope clutter distribution. This is a very common model for detection in the presence of chaff, sea clutter for pulse widths greater than 0.5 μs, sea clutter at grazing angles greater than 5°, land clutter observed from grazing angles greater than 5° over undeveloped terrain, and in any situation in which the clutter arises from a very large number of patches [2]. The exponential distribution family has a unit mean distribution given by [3]

$$F_u(x) = 1 - e^{-x} \tag{3}$$

The CFAR processor estimates the mean power, $\hat{\mu}_i$, of the interference in the i^{th} cell under test. The squared modulus of the cell under test is then compared to a threshold, T_i, where

$$T_i = C\hat{\mu}_i \tag{4}$$

and C is a constant controlling the probability of false alarm.

If the actual power in the cell under test exceeds the threshold in (4) then a detection is declared. If no errors are made in estimating the mean power μ_i, then the probability of false alarm, P_{FA}, assuming a unit mean distribution, $F_u(x)$, is

$$\begin{aligned} P_{FA} &= \int_C^\infty p_u(x)dx \\ &= 1 - \int_{-\infty}^C p_u(x)dx \\ &= 1 - F_u(C) \end{aligned} \tag{5}$$

where $p_u(x)$ is the probability density function of the interference power.

Hence the value of C which produces a desired false alarm probability of $P_{FA_{des}}$, with

exact mean estimation is,

$$C_0 = F_u^{-1}(1 - P_{FAdes}) \tag{6}$$

Thus for desired false alarm probabilities of $P_{FAdes} = 10^{-3}$, 10^{-4}, 10^{-6}, and 10^{-8}, and an exponential distribution, the optimal values of C may be computed as, $C_0 = 8.39$ dB, 9.64 dB, 11.40 dB and 12.65 dB respectively.

2.0 EVALUATING CFAR PERFORMANCE

In this report CFAR techniques are applied to a missile approach warning system (MAWS) radar mode. The system employs an airborne pulse-Doppler radar at an altitude of 100 m, with a pulse width of 3.33 μs and a pulse repetition frequency of 50 kHz. There are a total of five range gates (spaced 500 m apart), and 128 Doppler frequency bins.

The DREO airborne radar simulator (ABRSIM) [11-15] was used to generate the interference in the Doppler bin outputs of each range gate. The interference return to any individual range-Doppler cell is assumed to be a random variable, with all of the cells having the same distribution family, in this case exponential. The interference is composed of either thermal noise alone, or both ground clutter and thermal noise. Each snapshot of the ensemble of possible return signals contains 640 range-Doppler cells. To ensure statistical accuracy many independent snapshots of the range-Doppler map were generated.

The CFAR algorithm being tested is applied to each snapshot to estimate the mean power in each cell, $\hat{\mu}_i$. An estimation error for each cell is computed as the ratio $\hat{\mu}_i/\mu_i$, in which μ_i is the mean power of the cell taken over the ensemble of snapshots. The natural logarithm of the estimation error is computed for all of the cells in the ensemble of snapshots, and a global log-estimation-error histogram, $f_{ln(\hat{\mu}/\mu)}(x)$, is formed.

The system false alarm probability can be determined using this log-error histogram, the CFAR constant **C**, and knowledge of the distribution family. This results from the fact that P_{FA} is only dependent upon the ratio of the threshold and the mean power, not upon their actual values. Thus setting N equal to the number of cells, P_{FA} may be computed as follows [3].

$$\begin{aligned} P_{FA} &= \frac{1}{N}\sum_i \int_{-\infty}^{\infty} P(\ln T_i = x) P(\ln X_i > x)\, dx \\ &= \frac{1}{N}\sum_i \int_{-\infty}^{\infty} f_{\ln T_i}(x)(1 - F_{X_i}(e^x))\, dx \end{aligned} \tag{7}$$

$$P_{FA} = \frac{1}{N} \int_{-\infty}^{\infty} \sum_i f_{ln\left(\frac{\hat{\mu}_i}{\mu_i}\right)}(x - \ln C)(1 - F_u(e^x))dx$$
$$= \int_{-\infty}^{\infty} f_{ln\left(\frac{\hat{\mu}}{\mu}\right)}(x - \ln C)(1 - F_u(e^x))dx \quad (8)$$

Hence P_{FA}, as a function of $ln\ C$ is found by correlating the global log-error histogram with the function $1 - F_u(e^x)$. The log-error histogram need only be taken once, for $C = 1$, since the log-error histogram shifts to the right or left, depending upon the value of C. Determining the value of C which yields the desired probability of false alarm, P_{FAdes}, is a trial and error process which involves iterative solutions of (8). A bisection search algorithm was implemented to determine the value of C which yielded a false alarm probability within one one-thousandth of the desired probability of false alarm.

The different CFAR techniques all have different biases and variances, hence comparing only C values between the techniques is meaningless. By forming histograms of the estimated powers in each cell $\hat{\mu}_i$, a cumulative distribution function of the estimated powers can be found, $F_{est}(x)$. Once C has been computed using (8), the cumulative distribution function of the threshold can be found, using (4), from [16],

$$F_T(x) = F_{est}\left(\frac{x}{C}\right) \quad (9)$$

Comparison of the threshold distribution functions, $F_T(x)$, can be used to rate the performance of different CFAR techniques. If $F_T(x)$ for one CFAR method is strictly to the left (or above) of the $F_T(x)$ from another CFAR method, then the first algorithm is better because it will produce a smaller false alarm probability for any value of the return echo power. This is because the threshold will be larger for the first method than the second, resulting in a smaller false alarm rate. The horizontal distance between the threshold distributions is the difference in CFAR loss between the methods for a steady target at a detection probability of $P_D = F_T$. The absolute CFAR loss can be found by comparing $F_T(x)$ to the distribution of the thresholds for an ideal receiver, in which $T_i = C_0\mu_i$.

The probability of detection, P_D, of a target can be computed using the threshold distribution function $F_T(x)$. For a complex target, having a power density function $f_{P_t}(x)$, the detection probability is

$$P_D = \int_{-\infty}^{\infty} F_T(x) f_{P_t}(x) dx \quad (10)$$

and for a target with a steady power of P_T, the detection probability is

$$P_D = F_T(P_T) \tag{11}$$

A summary of the technique used to compare various CFAR algorithms concludes this section. First, many snapshots of the range-Doppler map are processed with the competing CFAR methods. Histograms are formed for both the logarithm of the estimation errors, and the estimated values themselves. A cumulative distribution function of the estimated values can then be constructed, by integrating the histogram of the estimated values. Next the value of the CFAR multiplying constant C is computed using (8) for the desired false alarm rate. Once the value of C has been determined, the threshold distribution function is obtained with (9). Finally, the threshold distribution functions of the competing CFAR algorithms are compared to determine the best method.

3.0 REFERENCE CELLS

The range-Doppler maps generated by the simulator, for the MAWS radar mode, contain five range gates and 128 Doppler bins. The interference powers in the range-Doppler map are identically distributed. In order to estimate the interference power in any particular test cell, the interference powers from a set of reference cells are used.

The target power is often divided between a small number of adjacent radar cells because the targets are not generally centred in a range gate or a doppler bin. Consequently, the range-Doppler cells which immediately surround the test cell are not included in the reference cell set. By excluding these cells, a guard cell region is developed which helps to prevent target self-masking from occurring [17]. Note that it is assumed that no additional targets are present in any of the reference cells.

The reference cell set may be one or two-dimensional. That is, cells in either range, Doppler, or range and Doppler dimensions may be included in the reference cell set. The notation that is used throughout this report first lists the number of range gates from which reference cells may be obtained and then lists the number of Doppler bins which contribute to the reference set of cells. Reference cells in the range dimension generally include an equal number of cells that are closer and farther in range than the test cell. Likewise, reference cells in the Doppler dimension include an equal number of cells with larger and smaller Doppler frequencies than the test cell. Hence a 4x0 reference window contains cells in the two range gates preceding the guard range gate closer than the test cell, and cells in the two range gates following the guard range gate immediately beyond the test cell. Figures 1 through 8 illustrate the test cell, guard cells, and reference cells for various reference window sizes and test cell positions. Note that a test cell which lies on the border of the range-Doppler map, will have fewer reference cells than one found in the centre of the map because some of the reference cells fall beyond the map's border. This is illustrated in Figures 1 and 2, and Figures 7 and 8.

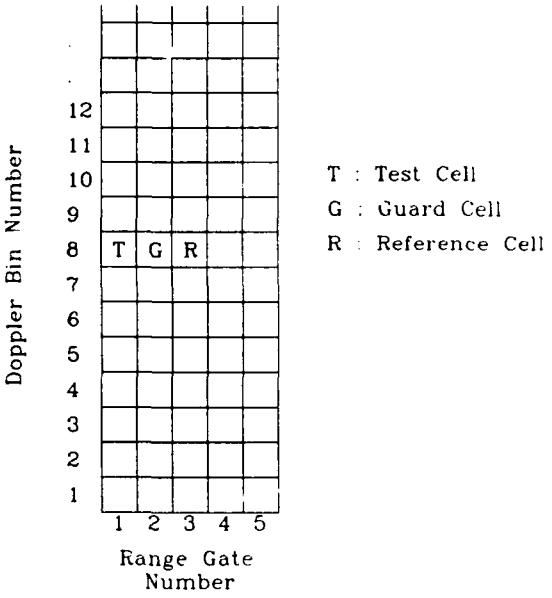

Figure 1 : 2 x 0 Window, Test Cell at (1,8)

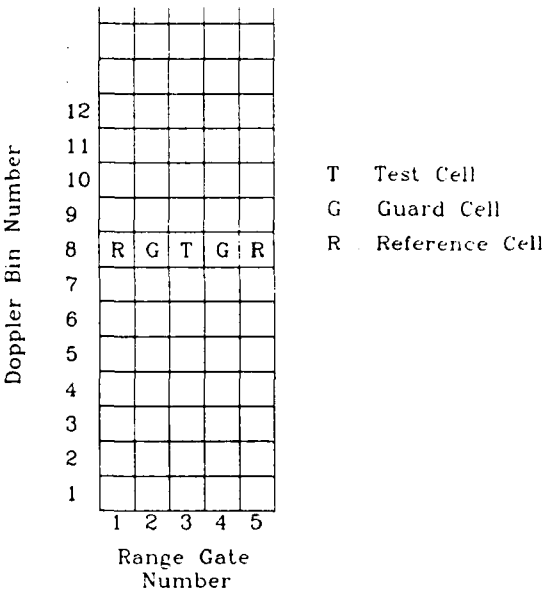

Figure 2 : 2 x 0 Window, Test Cell at (3,8)

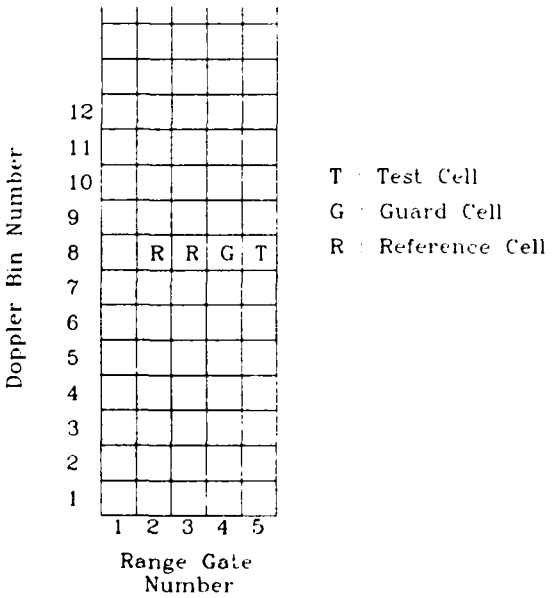

Figure 3 : 4 x 0 Window, Test Cell at (5,8)

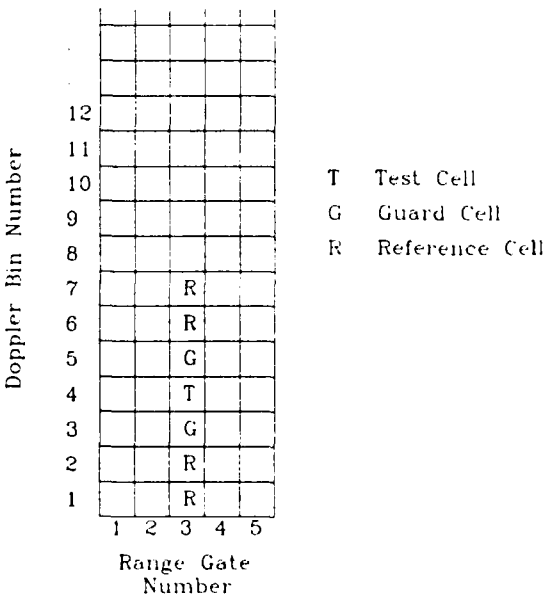

Figure 4 : 0 x 4 Window, Test Cell at (3,4)

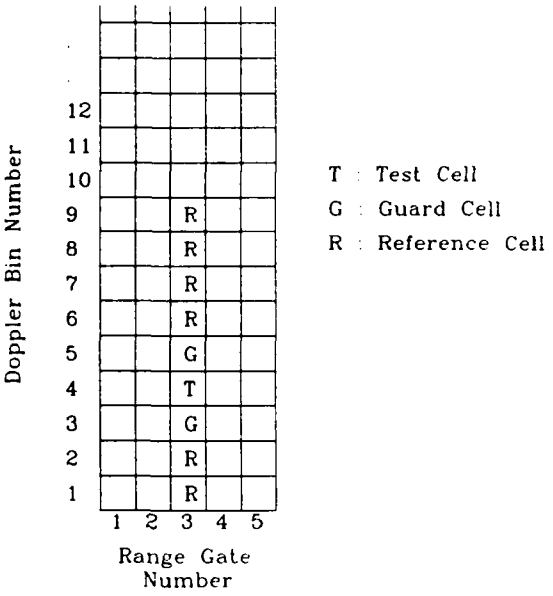

Figure 5 : 0 x 8 Window, Test Cell at (3,4)

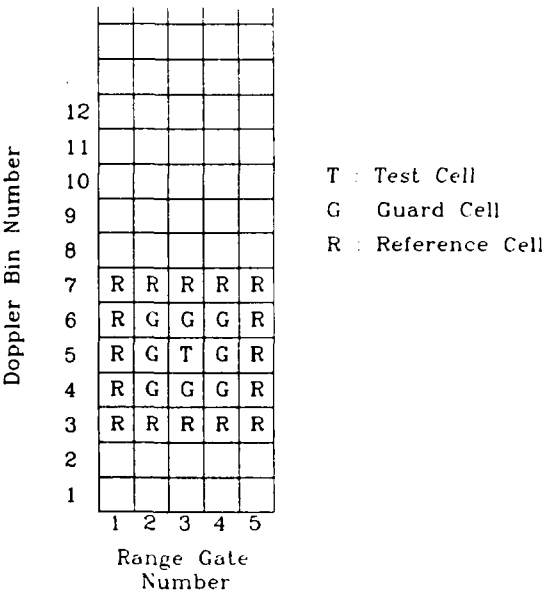

Figure 6 : 2 x 2 Window, Test Cell at (3,5)

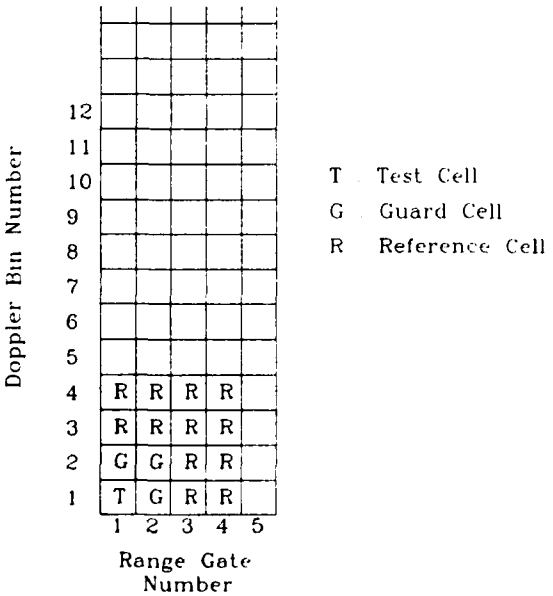

Figure 7 : 4 x 4 Window, Test Cell at (1,1)

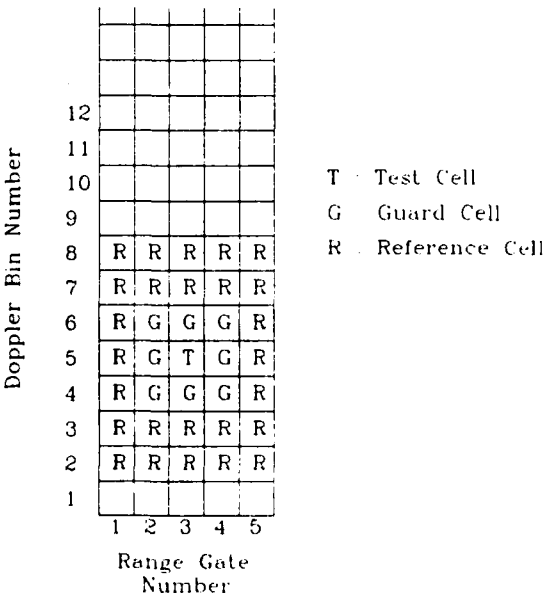

Figure 8 : 4 x 4 Window, Test Cell at (3,5)

4.0 CELL-AVERAGING (CA-) CFAR

A cell-averaging CFAR processor estimates the interference power in the cell under test by using the average value of the leading, trailing and surrounding reference cells. That is,

$$\hat{\mu}_i = \frac{1}{N}\sum_{j=1}^{N} X_j \tag{12}$$

where $\hat{\mu}_i$ is the estimated power of cell i, X_j is the power in reference cell j, and N is the size of the reference cell set. A block diagram of a one-dimensional CA-CFAR processor is given in Figure 9.

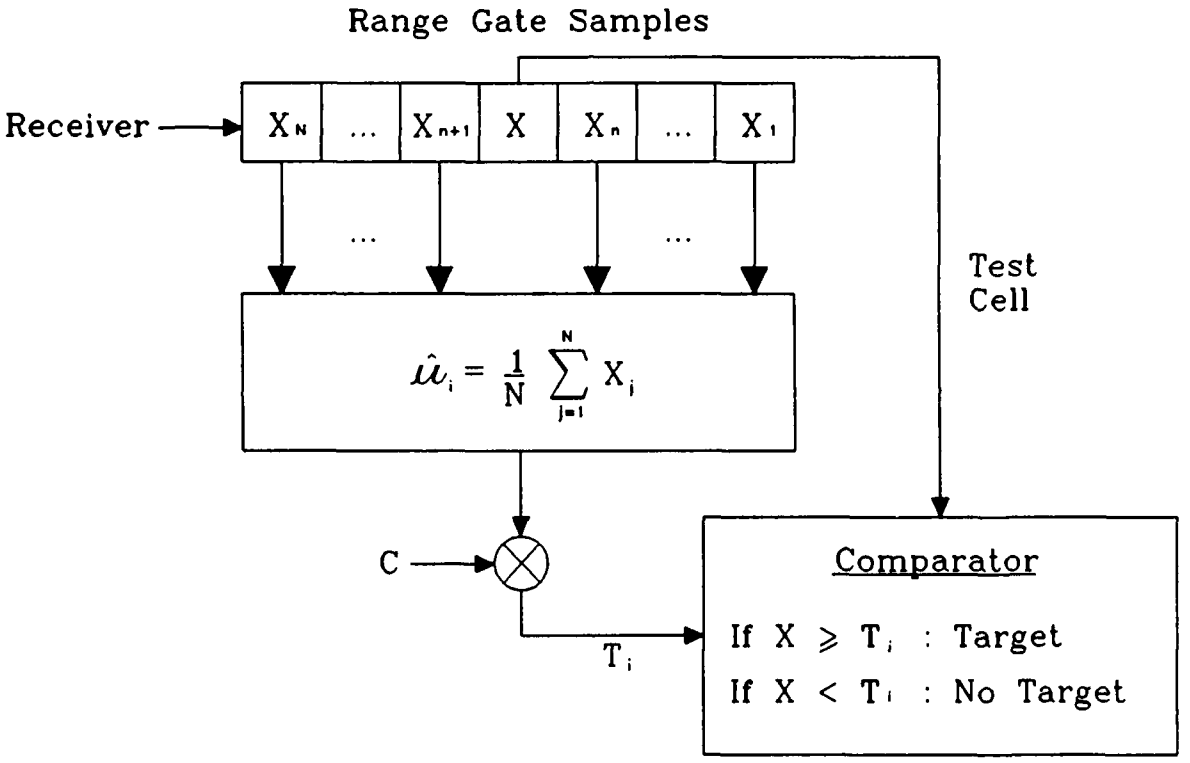

Figure 9 : Cell Averaging CFAR Processor

An inherent assumption of the CA-CFAR processor is that the interference statistics of each reference cell are identical to the statistics of the test cell. Consequently, the performance of the CA-CFAR processor deteriorates when the interference is nonhomogeneous over the reference cell window. The two most common forms of nonhomogeneity are edge effects and discrete scatterers [2].

Edge effects arise when the mean cell powers in the reference window undergo a step change along some boundary. This usually occurs when two or more different clutter environments (ie. land and sea) lie within the reference window.

Two different cases exist for edge effects [4]:

a) If the test cell lies in a region of weak interference, while some of the reference cells are immersed in the clutter edge then the threshold will be unnecessarily raised, thereby reducing the probability of detection, even though the cell under test has a high signal-to-noise ratio. The clutter regions are expanded by approximately half the length of the reference window, causing a masking effect to occur.

b) If the cell under test is immersed in the clutter edge, but some of the reference cells are in the clear region, then the probability of false alarm increases dramatically as the edge step size increases. This is a serious problem in the design of search radars [5].

The presence of a large discrete scatterer in one or more reference window cells can cause changes in the clutter distribution itself. This generally occurs when one or more interfering targets lie within the reference window. The resulting increase in the threshold level degrades the detection of the target in the cell under test.

5.0 GREATEST-OF (GO-) CFAR

The greatest-of CFAR processor is designed to combat the CA-CFAR problems which exist in the presence of interference edge effects. The GO-CFAR processor separates the reference window cells into two (or more) subsets based upon location. The average cell power in each subset is calculated and then the greatest average between the subsets is taken to be the estimated power of the cell under test. Hansen demonstrated that with this processor, the false alarm rate remains almost constant as the reference window moves over a clutter edge [5]. However, the masking effect discussed above is worsened. Figure 10 is an illustration of a one-dimensional (range only) GO-CFAR processor, in block format.

In the example of Figure 10, the subsets correspond to those cells which are closer in range than the cell under test, and those that are farther in range. In the two-dimensional averaging cases, cells at the same range, but smaller Doppler frequencies could be assigned to the first subset, while those with a larger Doppler frequency than the cell under test could be assigned to the second subset.

The GO-CFAR processor provides an improvement in the probability of false alarm, at a cost of a small additional loss in detection efficiency for detection in an interference distribution edge effect. However, the detection probability decreases severely when a single interfering target with strength equal to the test cell target appears in the reference window. The performance of GO-CFAR is worse than CA-CFAR for detection with target discrete scatterers [2].

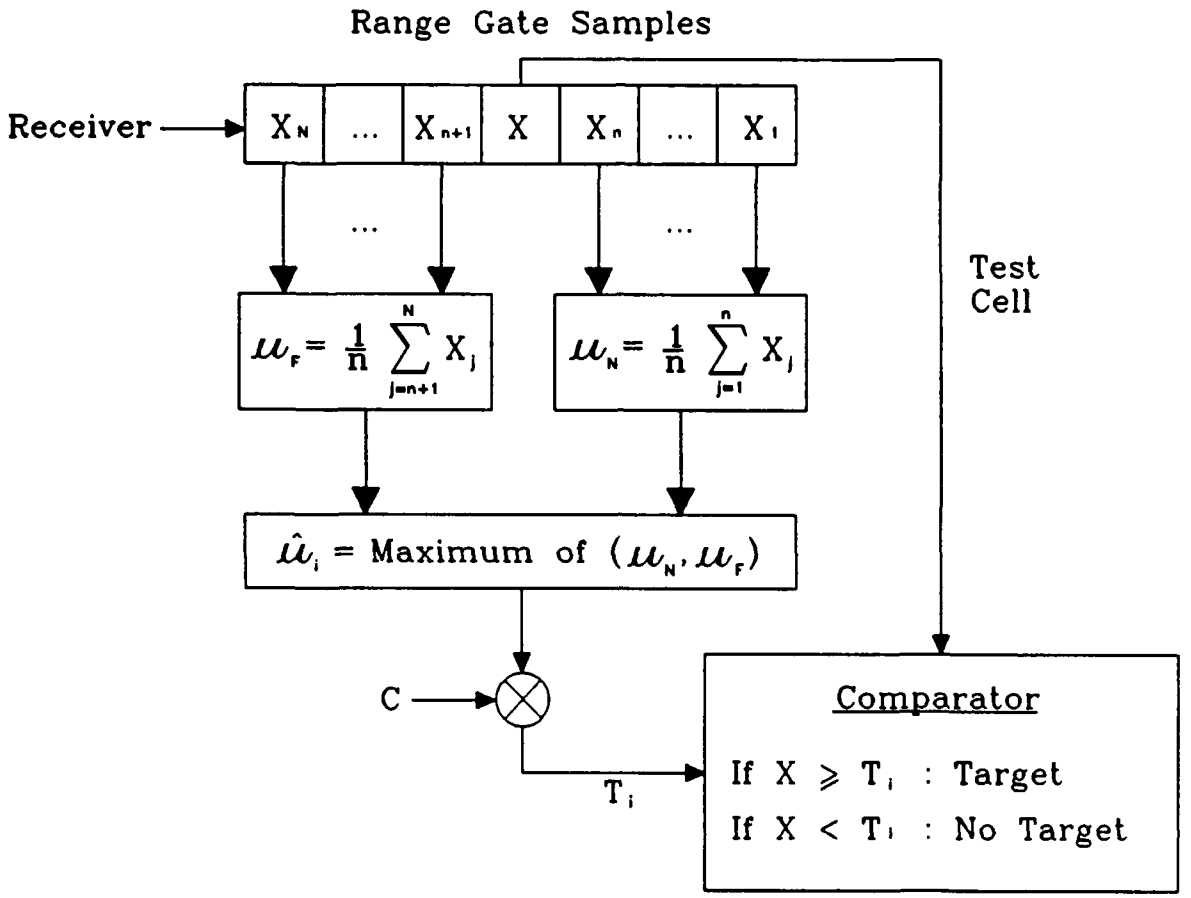

Figure 10 : Greatest - Of CFAR Processor

6.0 SMALLEST-OF (SO-) CFAR

A block diagram of a smallest-of CFAR processor, using a one-dimensional reference window, is illustrated in Figure 11.

The SO-CFAR processor forms reference cell subsets in the exact same manner as the GO-CFAR processor. However, rather than selecting the largest of the subset means, the SO-CFAR processor selects the smallest of the subset means, and assigns this quantity to the estimated power in the test cell.

The SO-CFAR processor performs significantly better than CA-CFAR for detection with one or more interfering targets in one half of the reference cell window. For detection with interfering targets in each half of the reference window the performance is similar to CA-CFAR. However, the SO-CFAR processor suffers severe degradation in false alarm rate control, as compared to CA-CFAR and GO-CFAR in the presence of an interference distribution edge effect in the reference cell window because of its tendency to underestimate the interference power [2].

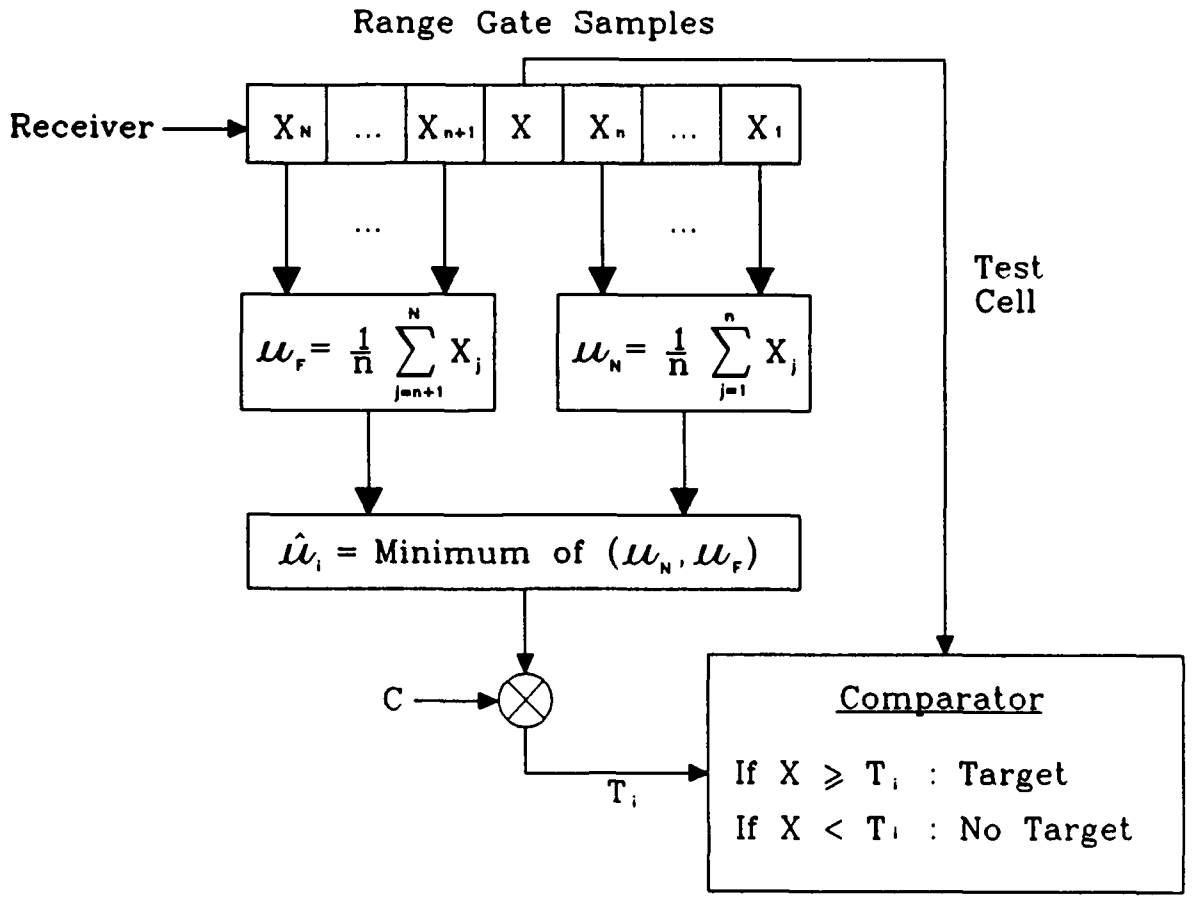

Figure 11 : Smallest - Of CFAR Processor

7.0 SIMULATION RESULTS

In this section the simulation results obtained using the three CFAR processors on two different types of interference, namely, thermal noise and thermal noise plus clutter are presented. The simple case of thermal noise interference is considered first.

7.1 Thermal Noise Interference

The thermal noise interference is assumed to be additive white Gaussian noise (AWGN) (consequently having an exponential power distribution). For this simulation, 100 snapshots of a 30 x 30 range-Doppler map were generated, resulting in a total of 90000 range-Doppler cells. The first two snapshots of the range-Doppler map are illustrated in Figures 12 and 13.

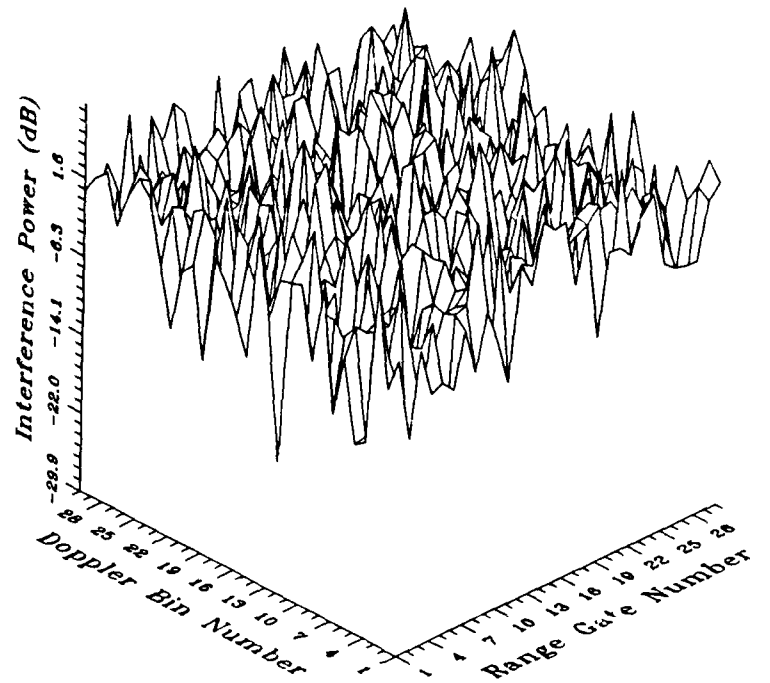

Figure 12 : Snapshot 1 - Noise Only

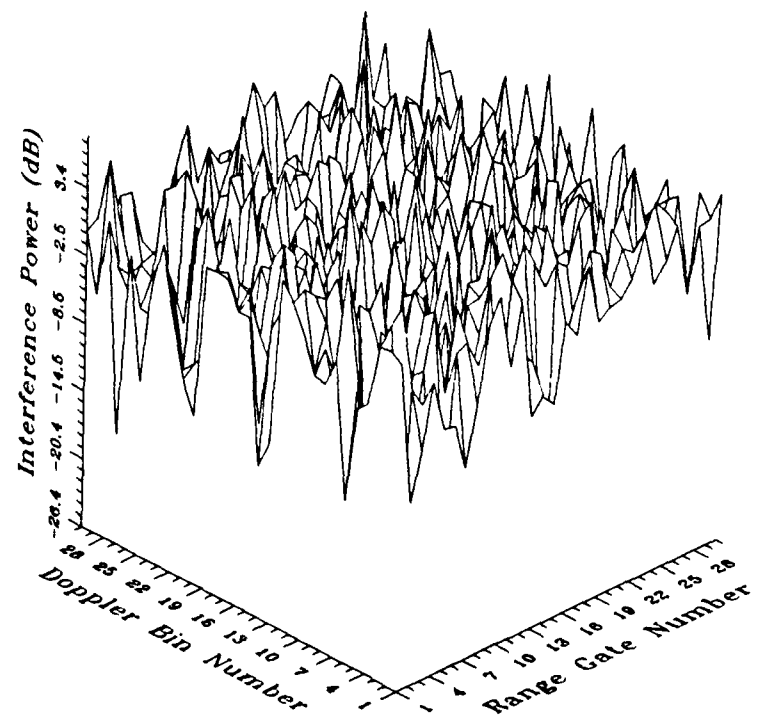

Figure 13 : Snapshot 2 - Noise Only

The generated noise had a mean power of 0.9985, or -0.0064 dB. This value was used in the computation of the log-error for each cell. The three different CFAR techniques were performed on the ensemble of maps, and the value of the threshold multiplier, **C**, was computed for desired false alarm rates of 10^{-3}, 10^{-4}, and 10^{-6}. The threshold multiplier was computed using reference window sizes of 2x2, 4x4, 8x8 and 16x16 in the range-Doppler dimensions. The results obtained are listed in Table 1.

Window Size	Desired P_{fa}	CA-CFAR		GO-CFAR		SO-CFAR	
		C (dB)	Actual P_{fa}	C (dB)	Actual P_{fa}	C (dB)	Actual P_{fa}
2 x 2	1. E-3	9.573	1.00 E-3	8.928	1.02 E-3	18.279	8.11 E-4
	1. E-4	11.298	4.44 E-5	10.685	7.78 E-5	29.143	9.99 E-5
	1. E-6	14.224	0.00	13.771	0.00	52.403	0.00
4 x 4	1. E-3	8.869	1.11 E-3	8.421	1.14 E-3	11.882	1.02 E-3
	1. E-4	10.291	1.11 E-4	9.865	9.99 E-5	17.865	9.99 E-5
	1. E-6	12.442	0.00	12.049	0.00	41.595	0.00
8 x 8	1. E-3	8.570	1.03 E-3	8.266	1.09 E-3	9.821	1.16 E-3
	1. E-4	9.881	1.22 E-4	9.592	1.33 E-4	14.761	1.22 E-4
	1. E-6	11.772	0.00	11.507	0.00	41.596	1.11 E-5
16 x 16	1. E-3	8.458	1.01 E-3	8.249	1.03 E-3	9.234	1.05 E-3
	1. E-4	9.730	1.22 E-4	9.530	1.22 E-4	14.408	1.44 E-4
	1. E-6	11.535	0.00	11.350	0.00	41.594	1.11 E-5

Table 1 : Simulation Results of the Noise-Only 30 x 30 Maps

In order to ensure that consistent estimates of **C** are obtained from the simulation, five different starting seeds for the random number generator were used for the 2x2 reference window case. The variation in the **C** values obtained for each false alarm rate, from the five different starting seeds are listed in Table 2. It is evident that for a false alarm rate of 10^{-3}, consistent (within fractions of a decibel) estimates of **C** are obtained for all three CFAR processors. For a false alarm rate of 10^{-4}, the CA and GO-CFAR processors had consistent estimates of **C**, but the SO-CFAR processor had a variation of approximately 1.5 dB over the five different starting seeds. The 10^{-6} false alarm rate caused a variation of 13.43 dB for SO-CFAR, 0.42 dB for GO-CFAR and 0.65 dB for CA-CFAR. The reason for the large variations in the SO-CFAR processor for smaller false alarm rates will become evident when the log-error

histograms are examined. As a result of these variations, depending upon the starting seed, all three CFAR processors shall only be compared for a false alarm rate of 10^{-3}. The CA and GO-CFAR processors can be accurately compared for $P_{fa} = 10^{-4}$, and an approximate relationship between these two processors can be obtained, with 100 snapshots for $P_{fa} = 10^{-6}$.

Desired P_{fa}	CA-CFAR (dB)	GO-CFAR (dB)	SO-CFAR (dB)
10^{-3}	0.0421	0.0483	0.4766
10^{-4}	0.1111	0.1015	1.5031
10^{-6}	0.6465	0.4178	13.4325

Table 2 : C Value Variation over 5 Different Starting Seeds for a 2 x 2 Reference Window

The CFAR algorithms were tested by comparing the threshold for each cell, in each snapshot (computed using (4)), to the actual cell power. Since there were no targets in any of the snapshots, a false alarm occurs whenever the actual cell power exceeds the threshold. In this manner, it is possible to count the number of false alarms, and hence compute an actual false alarm rate over the ensemble of snapshots. As evident from Table 1, the actual false alarm rate obtained was very close to the desired false alarm probability. Consequently, the method for computing the threshold multiplier, by using (8) is indeed validated. Note that while this testing method is not statistically accurate for a desired P_{fa} of 10^{-6} since only 90000 cells are used in the test, there are enough test cells to obtain a statistically meaningful value of P_{fa} for desired false alarm rates of 10^{-3} and 10^{-4}.

Because identical means and distributions were used for each cell, the CFAR performance should improve as the number of cells included in the reference window increases. The accuracy of the mean estimation increases as the number of cells used to form the estimated mean increases. Consequently, for a given reference window size, one would expect that the CA-CFAR processor should perform better than the GO-CFAR or SO-CFAR processors because it uses twice as many cells in estimating the mean power. We should also notice an improvement in the performance of any given technique, as the number of cells in the reference window is increased.

Figure 14 illustrates the log-error histogram obtained with the CA-CFAR processor for a reference window size of 4x4 range-Doppler cells. While the error density is centred at 0 dB, there is some residual error at -4.5 dB. It is this underestimation tail portion of the error density function that approximately defines the CFAR processor performance (recall that underestimating the interference power can dramatically increase the false alarm rate). The threshold multiplier, **C**, is an increasing function of the length of the negative tail (from 0 dB), and the desired false alarm rate [3].

The log error histogram for the 16x16 CA-CFAR processor is shown in Figure 15. Once again the error density function is centred at 0 dB. However, the variance in the distribution is much smaller than the distribution in Figure 14, because of the improvement in the accuracy of the mean estimation. This accuracy improvement is also illustrated by the decrease in the length of the underestimation tail, which is now about 1.4 dB.

The threshold distribution functions for the CA-CFAR processor, with four different window sizes, and desired false alarm probabilities of 10^{-3}, and 10^{-6} are illustrated in Figures 16 and 17, respectively. It is clear, from these figures, that as the number of reference cells increases, the performance of the CA-CFAR processor approaches the optimal threshold distribution, which is the vertical line plotted in the figures.

Figures 18 and 19 illustrate the log error histograms of the GO-CFAR processor for reference window sizes of 4x4 and 16x16 range-Doppler cells, respectively. The underestimation tails are approximately the same length as those of the CA-CFAR processor. The improvement in the estimation by using a 16x16 window is evident through the concentration of the error about the mean, and the smaller underestimation tail. However, it is evident from Figures 18 and 19 that a small positive bias is being imposed by the GO-CFAR processor. This bias manifests itself as a shift in the central portion of the distribution (approximately 0.5 dB for a 4x4 reference window). The bias occurs because GO-CFAR selects the greater mean of the two subsets, as opposed to CA-CFAR which selects the mean of the two subset means for the cell power estimation. Threshold distribution functions for the GO-CFAR processor are illustrated in Figure 20 for a false alarm rate of 10^{-3}, and Figure 21 for a false alarm rate of 10^{-6}. Again it is evident that the CFAR performance improves as the size of the reference window increases.

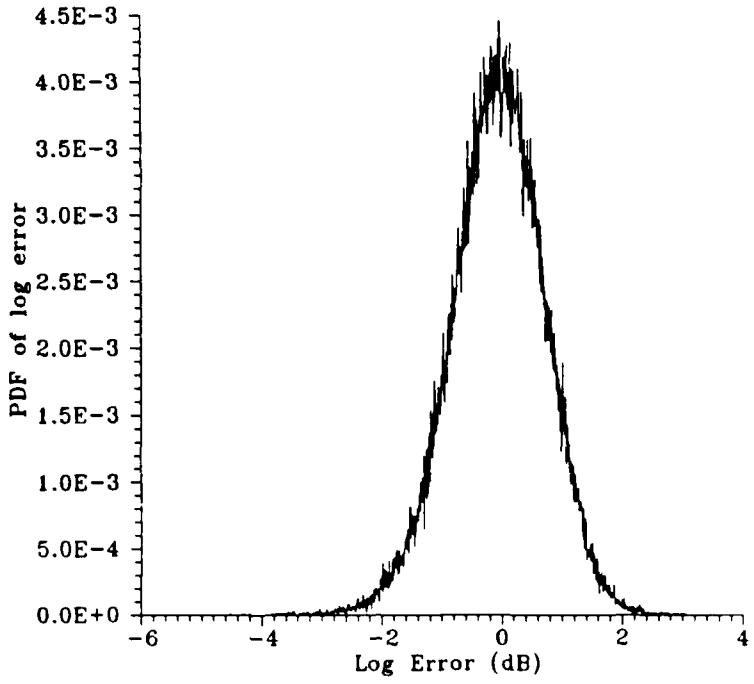

Figure 14 : Log-Error Histogram of CA-CFAR (4 x 4)

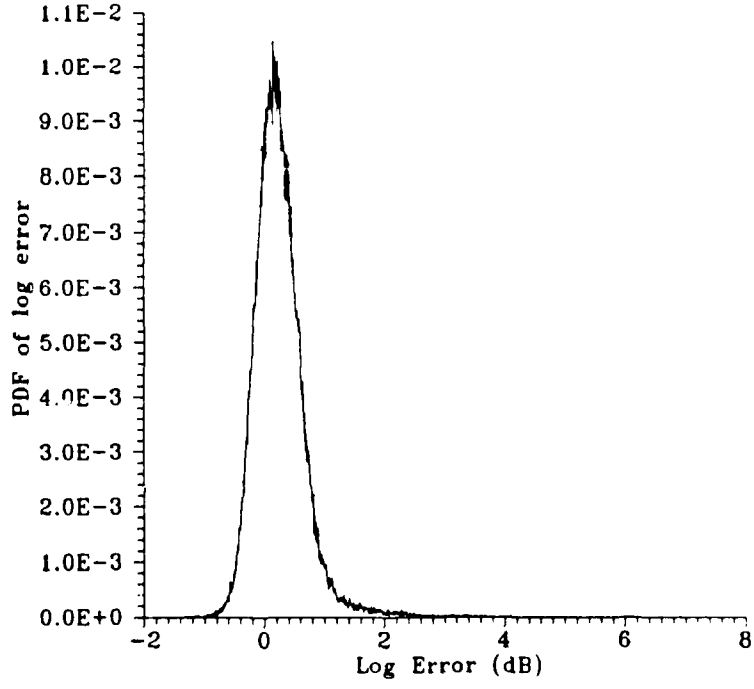

Figure 15 : Log-Error Histogram of CA-CFAR (16 x 16)

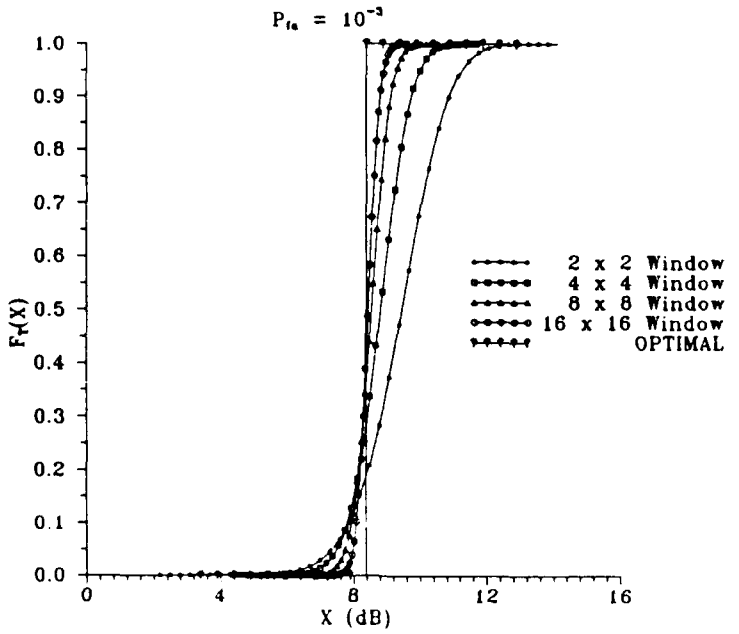

Figure 16: Threshold Distribution Functions for CA-CFAR in a Noise-Only Environment and $P_{fa} = 10^{-3}$.

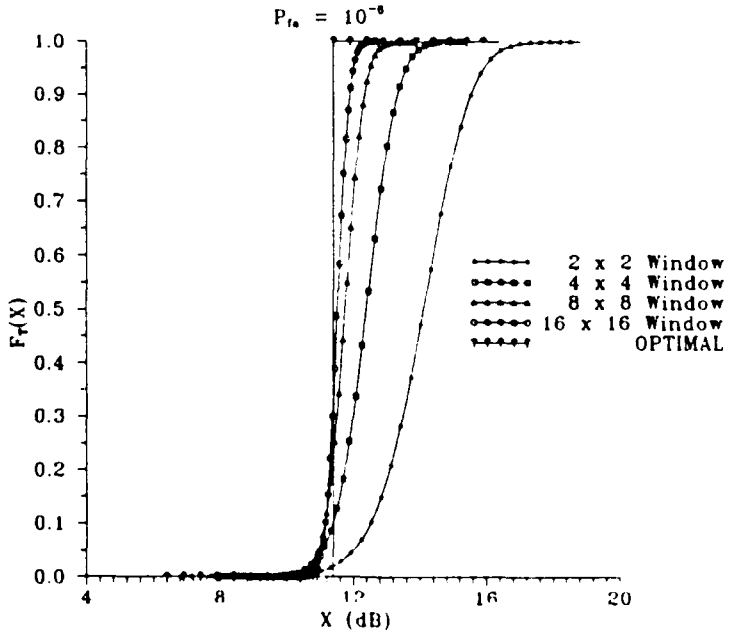

Figure 17: Threshold Distribution Functions for CA-CFAR in a Noise-Only Environment and $P_{fa} = 10^{-6}$.

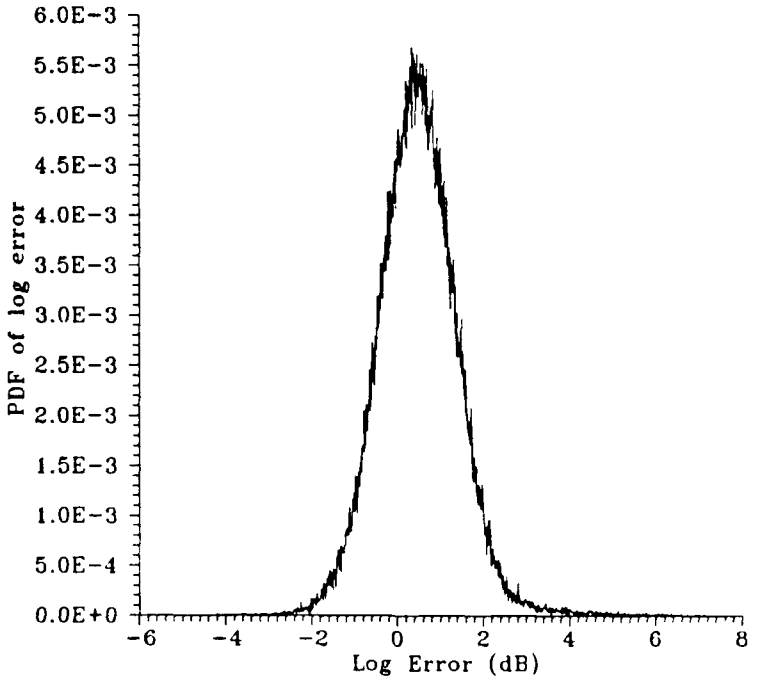

Figure 18 : Log-Error Histogram of GO-CFAR (4 x 4)

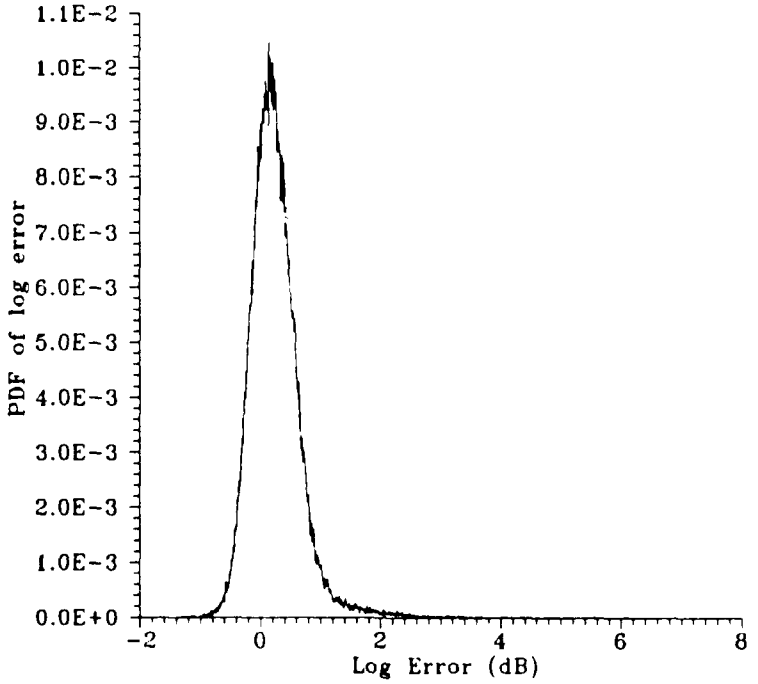

Figure 19 : Log-Error Histogram of GO-CFAR (16 x 16)

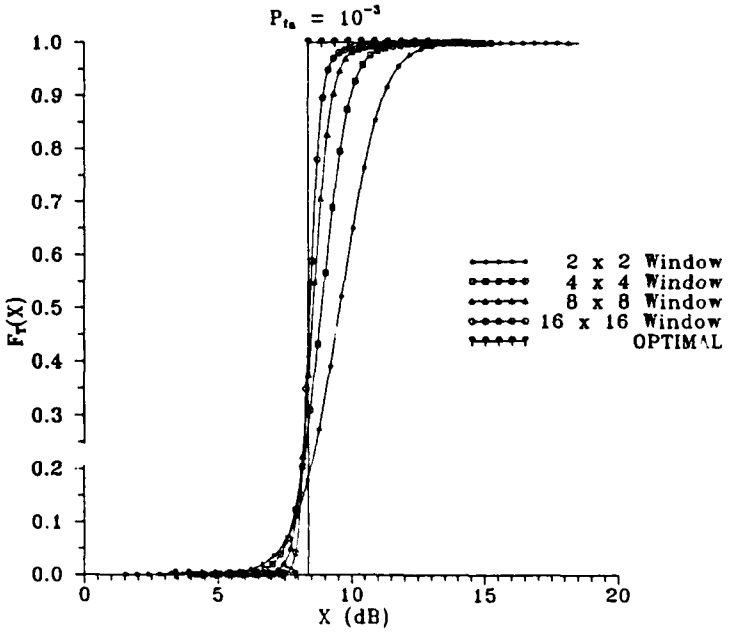

Figure 20: Threshold Distribution Functions of GO-CFAR in a Noise-Only Environment and $P_{fa} = 10^{-3}$.

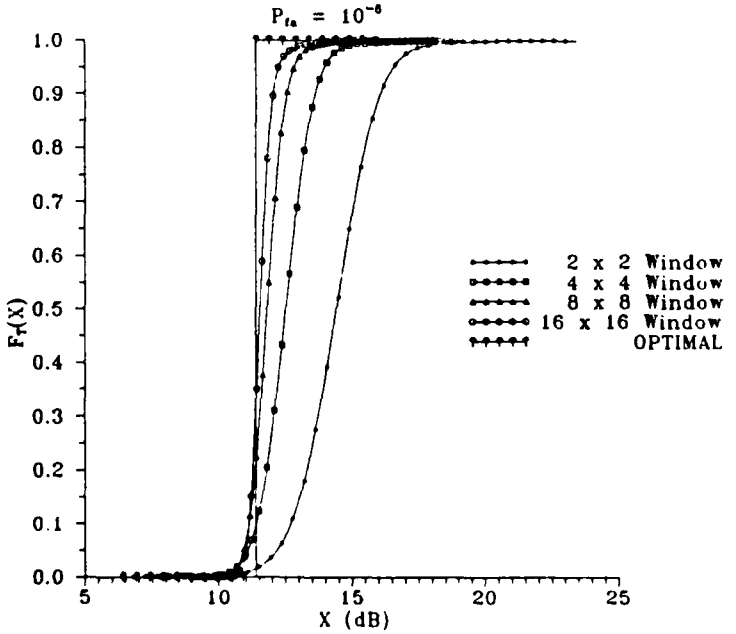

Figure 21: Threshold Distribution Functions of GO-CFAR in a Noise-Only Environment and $P_{fa} = 10^{-6}$.

Log-error histograms of the SO-CFAR processor with reference window sizes of 4x4 and 16x16 range-Doppler cells, are illustrated in Figures 22 and 23, respectively. Notice that the SO-CFAR processor produces very large underestimation tails (approximately 21 dB for a 4x4 window, and 20 dB for a 16x16 window), as a result of selecting the smaller mean of the two subsets. The smallest-of mean selection also produces a negative bias (about .75 dB for the 4x4 reference window) in the mean estimates. Figure 24 shows the resulting threshold distribution functions for a desired false alarm probability of 10^{-3}, and various window sizes. As the window size increases, the performance of the SO-CFAR processor improves.

The large underestimation tail produced by the SO-CFAR processor is the cause of the inconsistent estimates of the threshold constant, as the false alarm rate decreased, which was observed in Table 2. Recall that the threshold constant **C** is computed by correlating the log-error histogram with an exponential function. With 100 snapshots of the 30x30 maps the frequency of the log-error values in the edges of the underestimation tail is very small (often 1 or 2 out of 90000 samples). Because the underestimation tail's edge is correlated with the steep portion of the exponential function the resulting correlation is very sensitive to the frequency of the log-error values in the underestimation tail. As the false alarm rate decreases, the edges of the underestimation tail become more important in computing the threshold multiplier. Consequently, due to the small number of samples in the edge of this tail, a large variation in the value of **C** is observed as the false alarm rate becomes small. Many more snapshots of data are required to 'fill' this underestimation tail, so that consistent estimates can be obtained for small false alarm rates. By comparison, the underestimation tails of the CA and GO-CFAR processors were much smaller than the SO-CFAR processor, hence 100 snapshots were adequate to obtain consistent estimates of **C**.

By comparing the threshold distribution functions, shown in Figures 16, 17, 20, 21, and 24, it is evident that the CA-CFAR processor outperforms the GO-CFAR processor which in turn outperforms the SO-CFAR processor, for a given reference window size. In Figure 25 the threshold distribution functions of each processor are plotted using a 16x16 window size for a desired false alarm probability of 10^{-3}. Figures 26 and 27 illustrate the threshold distribution functions of the CA and GO-CFAR processors for false alarm rates of 10^{-4}, and 10^{-6}, respectively. These graphs highlight the superiority of the CA-CFAR processor over GO-CFAR, and the inferiority of the SO-CFAR processor versus GO-CFAR. The poor performance of the SO-CFAR processor, with respect to the other processors, could be predicted by its much longer underestimation tail in the log-error histograms. The underestimation bias of the SO-CFAR processor causes problems in this noise-only environment since underestimation of the mean power can greatly increase the false alarm probability.

For a steady target, a false alarm rate of 10^{-3}, a 16x16 reference window, and a detection probability of 0.5, the CFAR losses of the CA, GO and SO-CFAR processors were 0.05 dB, 0.06 dB, and 0.58 dB, respectively. Increasing the detection probability to 0.9 increased the CFAR losses to 0.44 dB, 0.56 dB, and 1.01 dB for the CA, GO and SO-CFAR processors, respectively. The CFAR losses of the CA and GO-CFAR processors remained essentially constant as the false alarm rate was decreased to 10^{-6}.

In summary, the histograms and threshold distribution functions which have been presented confirm the proper operation of the CFAR simulation, and illustrate the following trends. First, as the value of the threshold multiplier, **C**, increases, the false alarm rate decreases for any constant reference window size. Second, for a constant false alarm rate, the value of the threshold multiplier (and hence the CFAR loss) decreases as the reference window size increases. Third, as one would expect, the CA-CFAR processor outperforms the SO and GO-CFAR processors, for any particular window size, because it uses twice as many cells in estimating the mean power. Finally, because the SO-CFAR processor underestimates the mean power, its performance is much worse than either the CA or GO-CFAR processors.

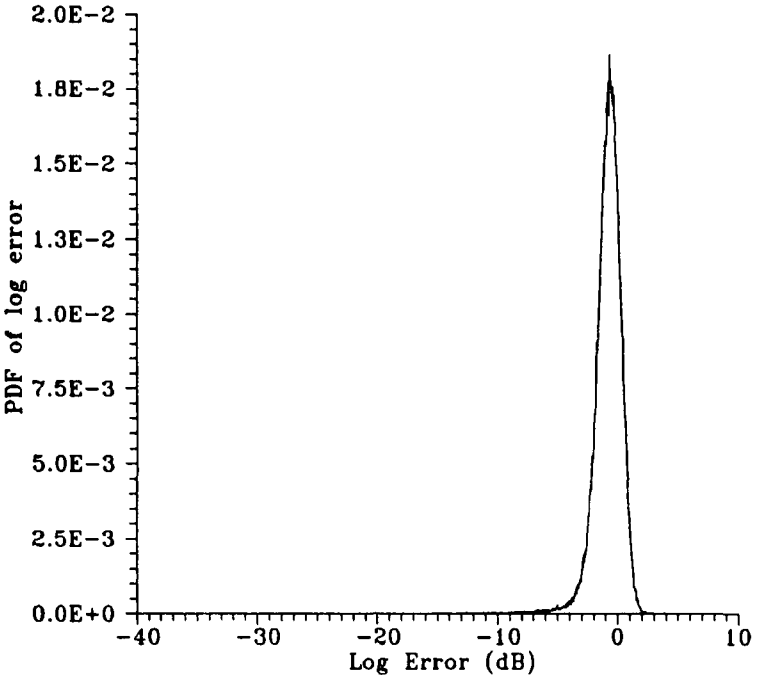

Figure 22 : Log-Error Histogram of SO-CFAR (4 x 4)

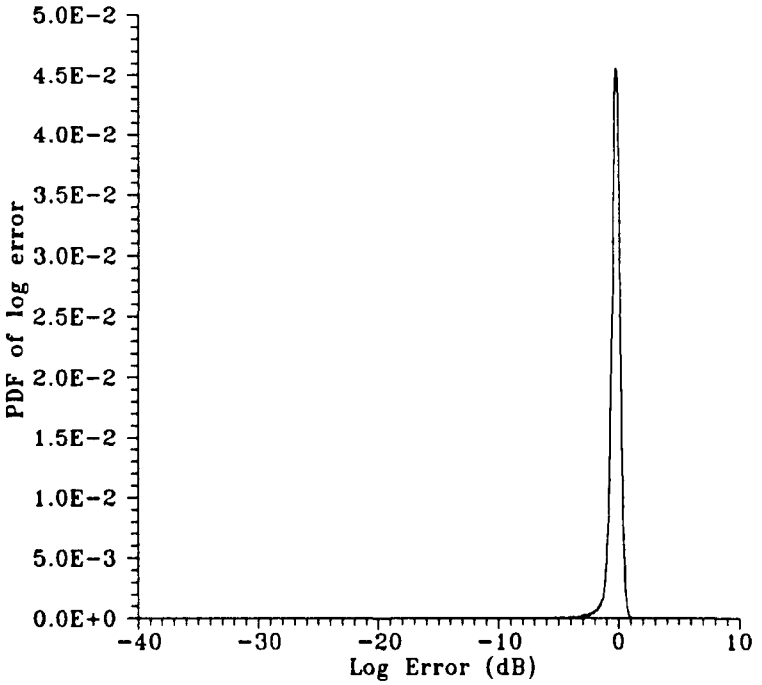

Figure 23 : Log-Error Histogram of SO-CFAR (16 x 16)

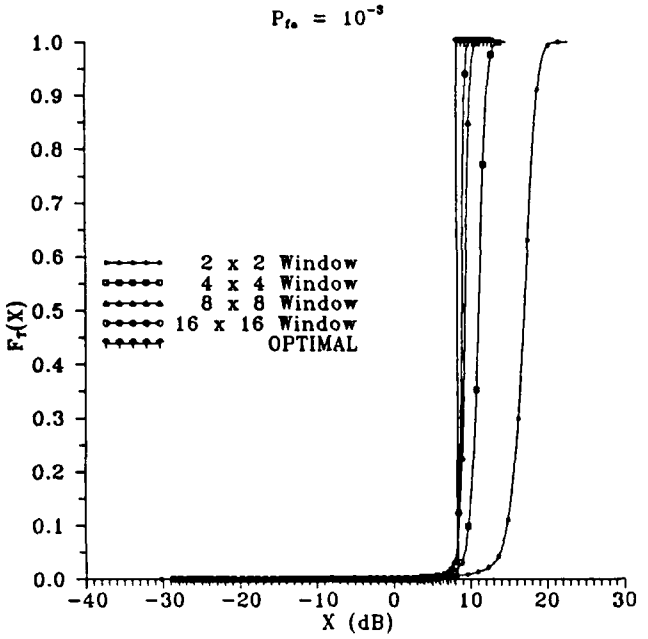

Figure 24: Threshold Distribution Functions of SO-CFAR in a Noise-Only Environment and $P_{fa} = 10^{-3}$.

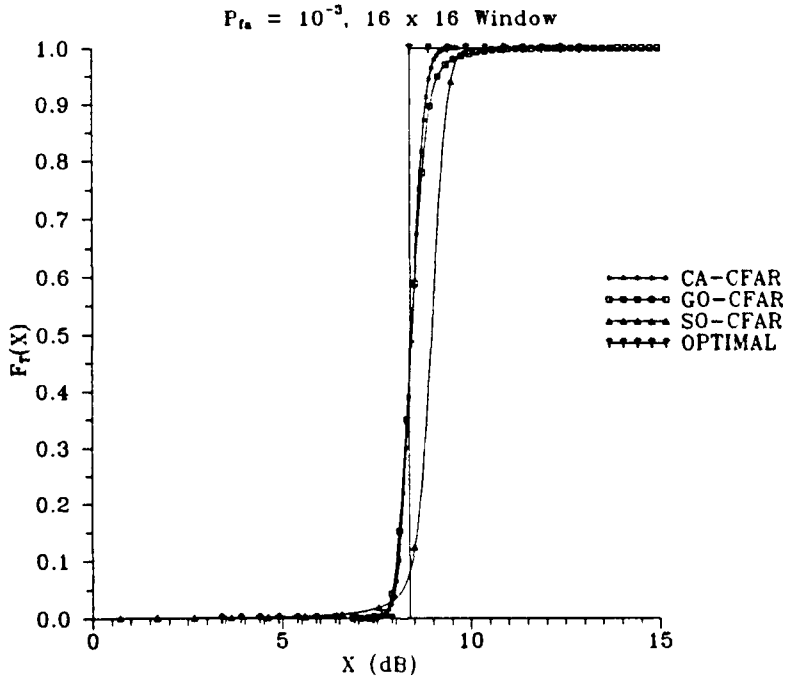

Figure 25 : Threshold Distribution Functions, Noise-Only

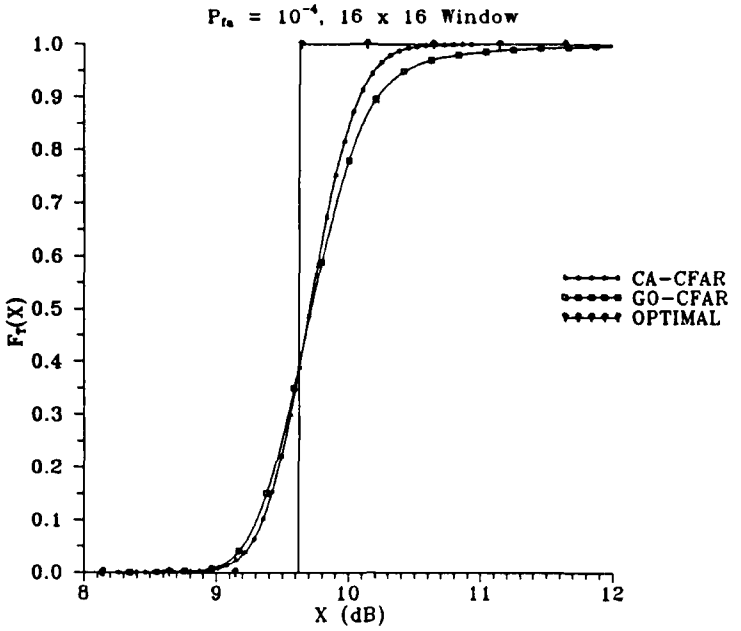

Figure 26 : CA and GO-CFAR (16x16) Threshold Distribution Functions, $P_{fa} = 10^{-4}$.

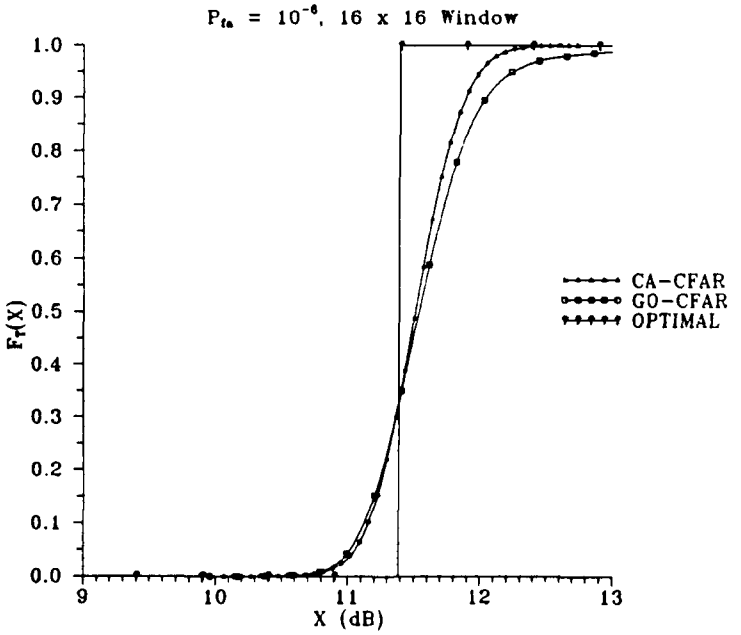

Figure 27 : CA and GO-CFAR (16x16) Threshold Distribution Functions, $P_{fa} = 10^{-6}$.

7.2 Clutter and Thermal Noise Interference

As mentioned earlier, the DREO airborne radar simulator was used to generate the interference power in the range-Doppler cells for a MAWS radar. One hundred snapshots of the 5 x 128 range-Doppler maps were produced. The interference power in each cell was an exponentially distributed variable, comprised of ground clutter and thermal noise. Figure 28 illustrates the mean values, over the ensemble of snapshots, of each range-Doppler cell. These values were used to compute the log-error function. Two different snapshots of the 5 x 128 maps are illustrated in Figures 29 and 30.

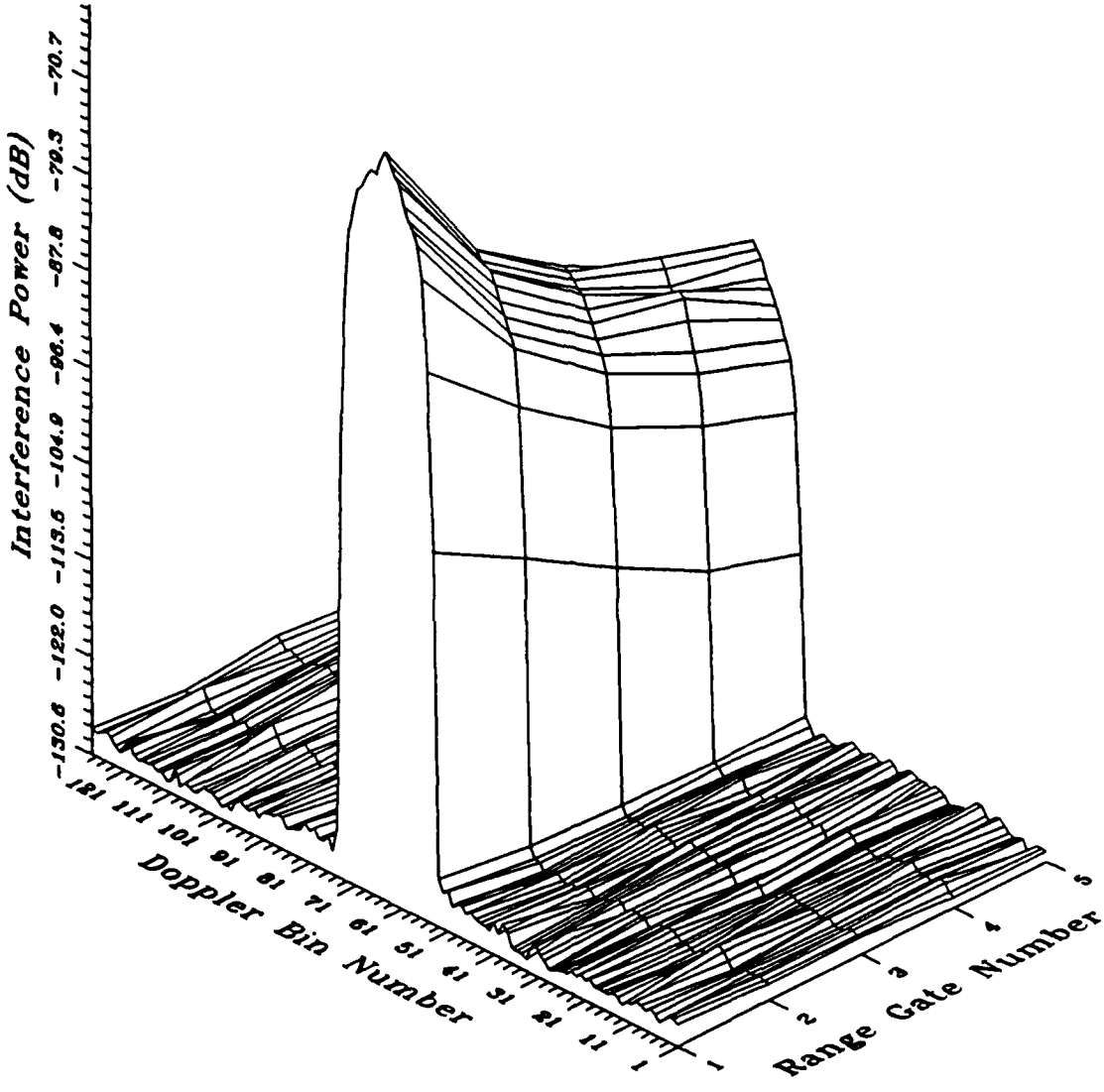

Figure 28 : Mean Range-Doppler Map, Clutter and Noise Environment

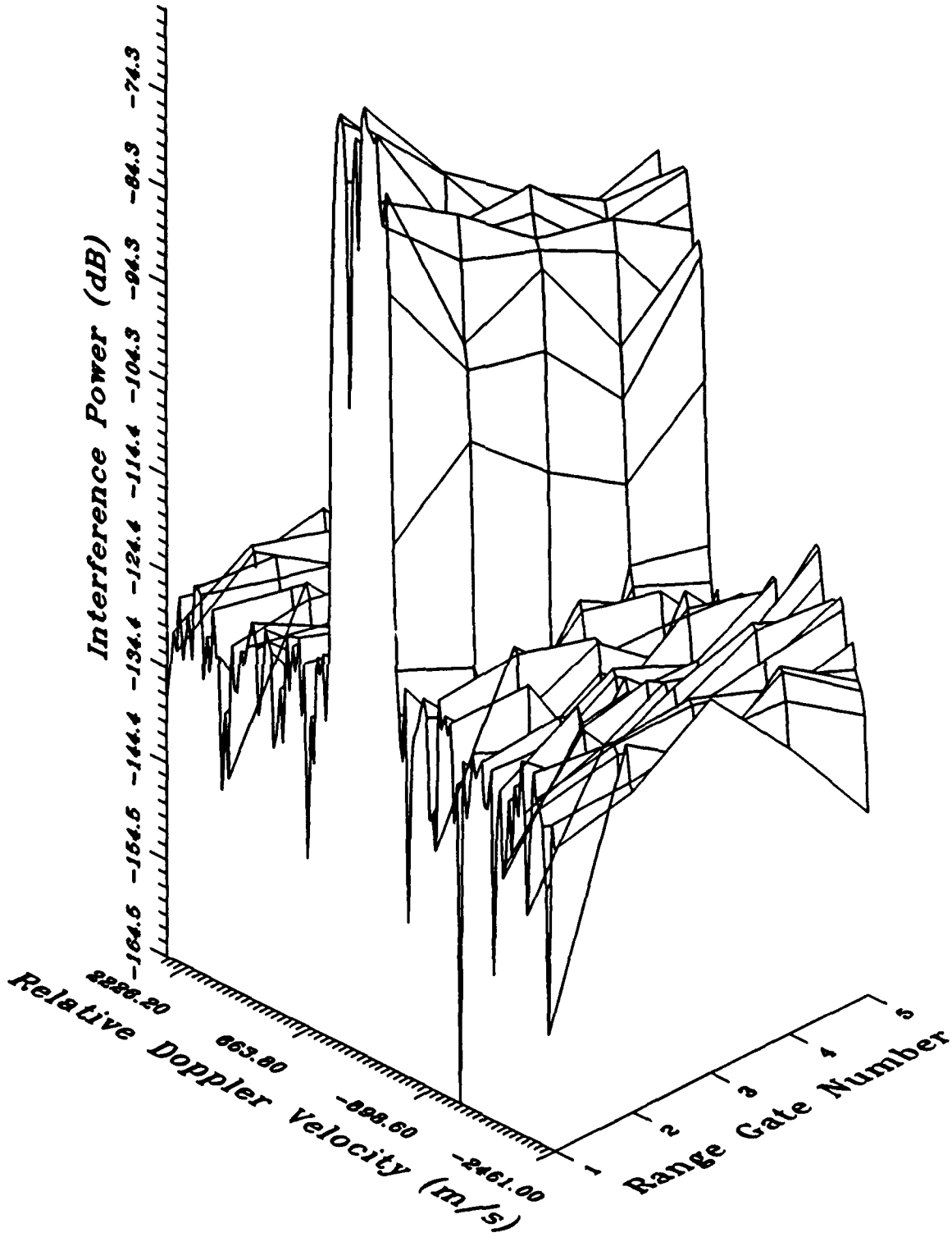

Figure 29 : Snapshot #1, Clutter and Noise Environment

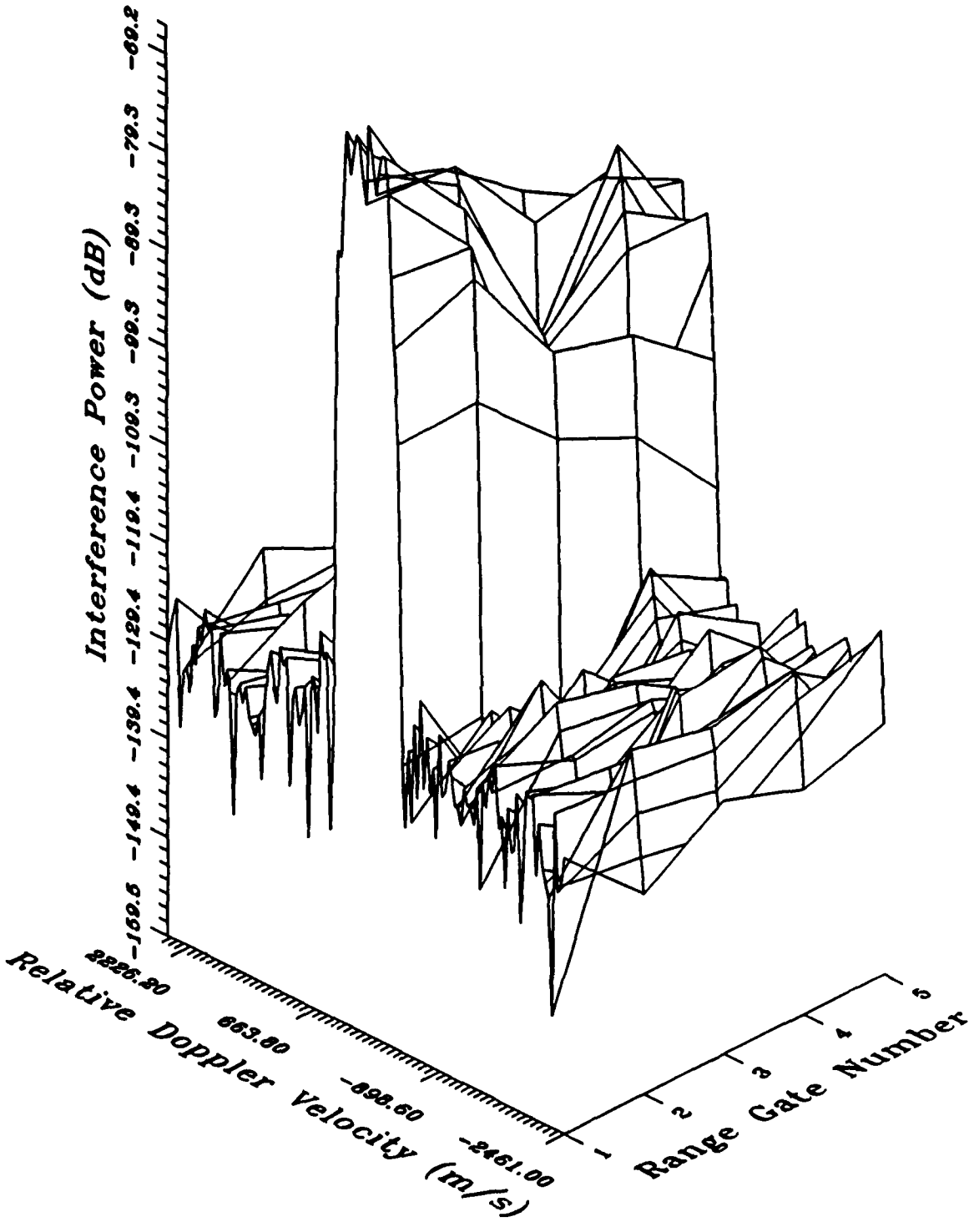

Figure 30 : Snapshot #2, Clutter and Noise Environment

By examining Figures 28 to 30 the difficulties which clutter impose on a CFAR algorithm become evident. Note that the interference includes contributions from the antenna's sidelobes and backlobes. There is a very large peak (approximately 60 dB) which extends throughout all five range gates between Doppler bins 50 and 80 (approximately $\pm$500 m/s). This peak is caused by the reflections of the transmitted radar pulses from the ground patches. Outside of this clutter peak region the range-Doppler map is quite 'flat' and the interference is mainly composed of thermal noise. Hence one would expect that the CFAR processor should be able to operate well in the noise portion of the map, but may have difficulty in the clutter dominated region.

The three CFAR processors were tested on all of the clutter maps. The effects of various reference window sizes, in one and two dimensions, were considered. The results, for desired false alarm probabilities of 10^{-3}, 10^{-4}, and 10^{-6} are listed in Table 3. As before, the computed value of **C** was tested by counting the number of false alarms that occurred over the ensemble of snapshots. The resulting 'actual' false alarm rate is also listed in Table 3. The actual value of the false alarm rate obtained is very close to the desired rate, hence, again the method for computing the threshold multiplier is validated. Note that all of the false alarms that did occur were from cells which were contained within the clutter peak region.

Window Size	Desired P_{fa}	CA-CFAR		GO-CFAR		SO-CFAR	
		C (dB)	Actual P_{fa}	C (dB)	Actual P_{fa}	C (dB)	Actual P_{fa}
2 x 0	1. E-3	34.207	9.68 E-4	34.205	9.69 E-4	34.911	9.53 E-4
	1. E-4	44.067	9.38 E-5	44.068	9.38 E-5	44.461	1.09 E-4
	1. E-6	51.853	0.00	51.853	0.00	51.908	0.00
4 x 0	1. E-3	28.724	1.08 E-3	28.724	1.08 E-3	30.049	1.14 E-3
	1. E-4	33.844	4.68 E-5	33.844	4.69 E-5	37.272	6.25 E-5
	1. E-6	41.731	0.00	41.731	0.00	49.114	0.00
6 x 0	1. E-3	28.646	9.06 E-4	28.648	9.06 E-4	29.843	1.00 E-3
	1. E-4	32.810	6.25 E-5	32.808	6.25 E-5	36.689	7.80 E-5
	1. E-6	39.010	0.00	39.009	0.00	49.115	0.00
0 x 2	1. E-3	19.695	8.13 E-4	18.595	7.50 E-4	50.979	8.28 E-4
	1. E-4	28.617	3.13 E-5	27.999	3.12 E-5	61.383	1.09 E-4
	1. E-6	39.476	0.00	39.387	0.00	75.421	0.00
0 x 4	1. E-3	14.432	5.31 E-4	13.504	5.62 E-4	48.667	8.90 E-4
	1. E-4	17.973	3.12 E-5	17.284	3.13 E-5	55.995	9.38 E-5

Window Size	Desired P_{fa}	CA-CFAR		GO-CFAR		SO-CFAR	
		C (dB)	Actual P_{fa}	C (dB)	Actual P_{fa}	C (dB)	Actual P_{fa}
0 x 4	1. E-6	23.876	0.00	23.465	0.00	63.116	0.00
0 x 8	1. E-3	12.254	7.19 E-4	11.403	7.50 E-4	48.068	9.37 E-4
	1. E-4	14.990	6.25 E-5	14.383	7.80 E-5	54.176	7.81 E-5
	1. E-6	19.632	0.00	19.312	0.00	60.294	0.00
0 x 16	1. E-3	11.313	6.40 E-4	10.395	5.93 E-4	47.820	9.06 E-4
	1. E-4	13.714	7.80 E-5	12.892	6.25 E-5	53.386	1.25 E-4
	1. E-6	17.325	0.00	16.683	0.00	58.819	0.00
0 x 40	1. E-3	14.526	7.34 E-4	13.345	5.90 E-4	48.232	8.12 E-4
	1. E-4	17.250	4.68 E-5	16.303	1.09 E-4	53.355	1.09 E-4
	1. E-6	20.953	0.00	20.108	0.00	58.183	0.00
2 x 2	1. E-3	14.998	7.50 E-4	12.396	9.06 E-4	42.687	1.02 E-3
	1. E-4	19.293	6.25 E-5	17.633	9.38 E-5	54.812	1.09 E-4
	1. E-6	24.823	1.56 E-5	24.163	1.56 E-5	70.972	0.00
4 x 4	1. E-3	14.949	8.13 E-4	11.417	8.90 E-4	42.470	1.09 E-3
	1. E-4	18.660	4.69 E-5	15.840	6.25 E-5	52.854	4.69 E-5
	1. E-6	23.611	0.00	21.991	0.00	61.001	0.00
6 x 6	1. E-3	15.322	8.43 E-4	11.239	9.69 E-4	42.366	9.22 E-4
	1. E-4	18.908	1.09 E-4	15.455	6.25 E-5	52.179	7.81 E-5
	1. E-6	23.225	0.00	21.347	0.00	60.280	0.00
2 x 16	1. E-3	12.973	1.02 E-3	10.265	8.59 E-4	43.112	9.53 E-4
	1. E-4	16.434	7.80 E-5	14.012	1.09 E-4	51.213	6.25 E-5
	1. E-6	20.574	0.00	18.839	0.00	57.025	0.00

Table 3 : Simulation Results of the Noise and Clutter 5 x 128 Maps

Log-error histograms of the CA-CFAR processor and reference window sizes of 4x0, 0x4, and 4x4 are illustrated in Figures 31 to 33, respectively. When averaging only in the range dimension (Figure 31) the length of the underestimation tail is approximately 36 dB. Averaging only in the Doppler dimension (Figure 32) reduces the underestimation tail to 18 dB, while using both the range and Doppler dimensions (Figure 33) produces a similar underestimation tail approximately 18 dB long. Based upon these histograms, we can predict that the 0x4 and 4x4 reference windows should provide similar performance, followed by the 4x0 reference window. Also note that the main peak in each of the CA-CFAR histograms is centred at 0 dB, indicating that CA-CFAR does not bias the estimated mean powers.

In Figures 34 to 36 the log-error histograms for a GO-CFAR processor with reference windows of 4x0, 0x4 and 4x4 are displayed. In each case the length of the underestimation tail is approximately the same as for the CA-CFAR processor. Consequently one should not expect much of a difference in the performance of these two CFAR processors. As in the noise-only environment, the GO-CFAR processor imposes a positive bias in the mean estimation which manifests itself as a slight shift to the right of the main peak in the log-error histogram.

Finally, the SO-CFAR processor's log-error histograms for reference windows of 4x0, 0x4, and 4x4 are displayed in Figures 37 to 39. From these figures one can see that the SO-CFAR processor inflicts a negative (underestimating) bias upon the estimated mean values. This processor also has a much longer underestimating tail than either the CA or GO-CFAR processors. The tail is approximately 42 dB for a 4x0 window, 59 dB for a 0x4 window, and 52 dB for a 4x4 window. Consequently, the performance of the SO-CFAR processor should not be very good relative to the CA or GO-CFAR processors.

As in the thermal noise environment, the frequency of the log-errors in the edge of the underestimation tail is very small for the SO-CFAR processor. This means that the values of the threshold multiplier, **C**, obtained from (8), will not be consistent for small values of the false alarm rate. Many more snapshots are required to obtain accurate results for the value of **C** for false alarm rates of 10^{-4}, and 10^{-6}. Hence, the SO-CFAR threshold distributions will only be plotted for a false alarm rate of 10^{-3}.

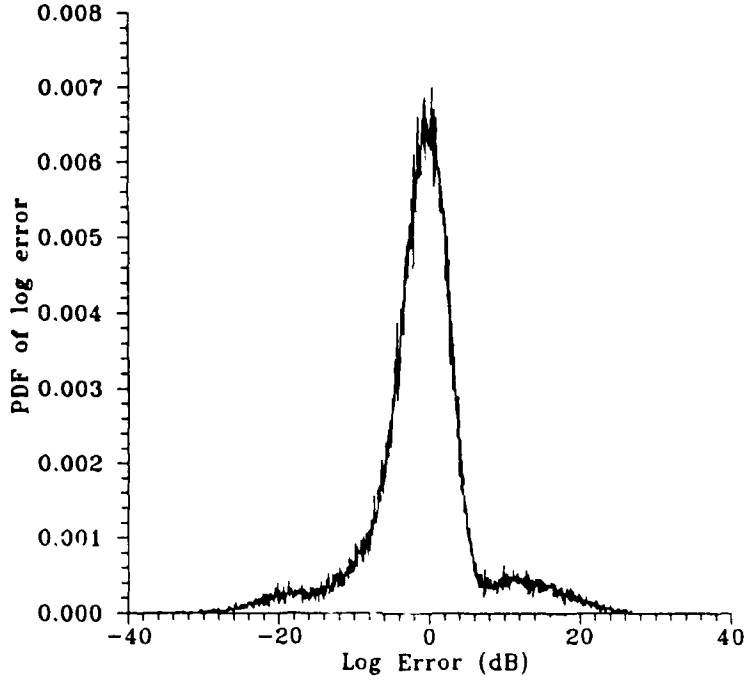

Figure 31 : Log-Error Histogram of CA-CFAR (4 x 0)

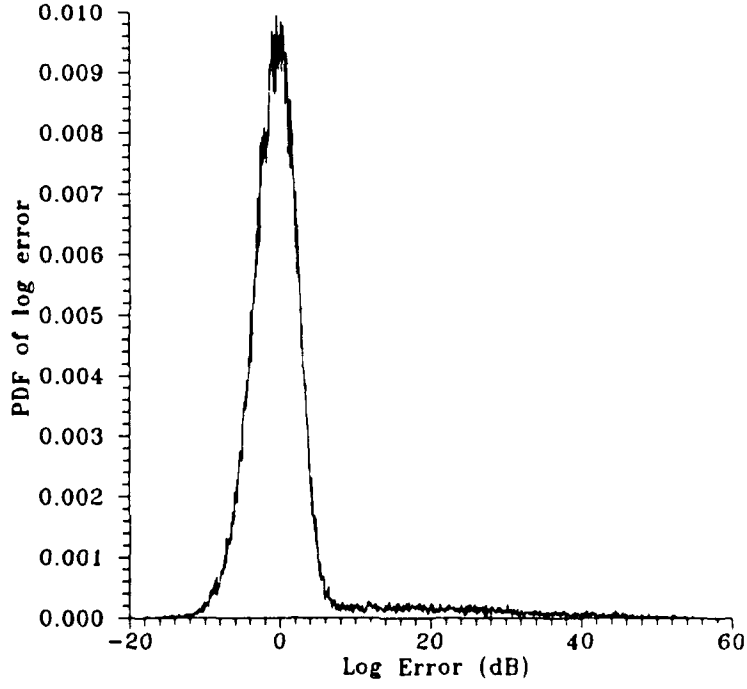

Figure 32 : Log-Error Histogram of CA-CFAR (0 x 4)

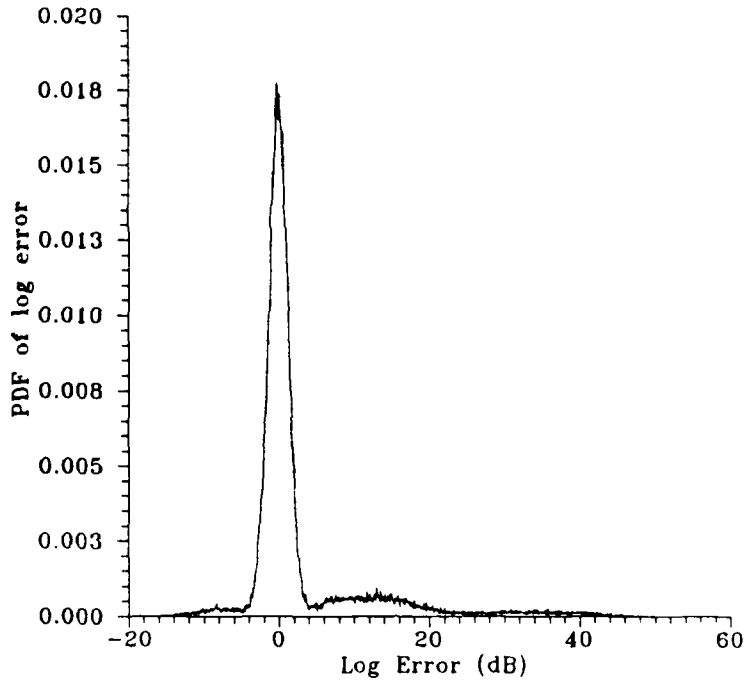

Figure 33 : Log-Error Histogram of CA-CFAR (4 x 4)

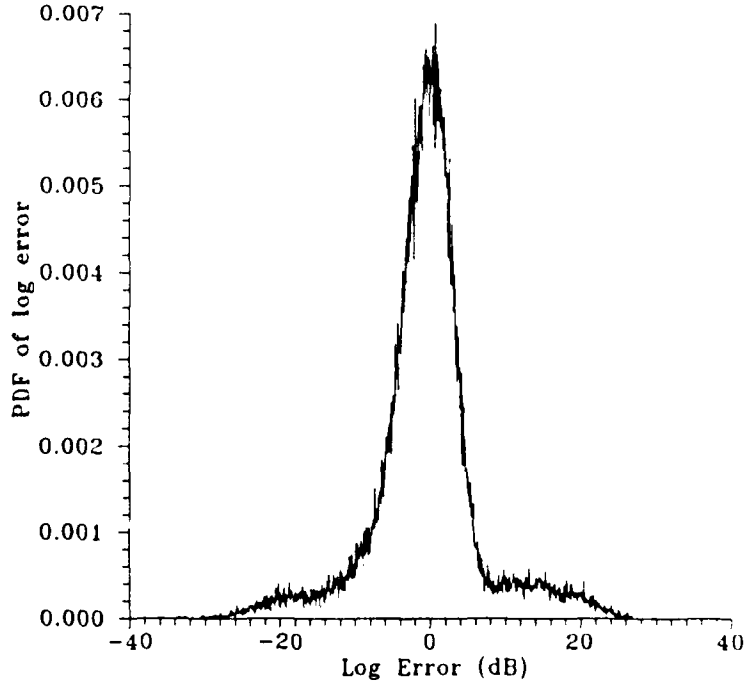

Figure 34 : Log-Error Histogram of GO-CFAR (4 x 0)

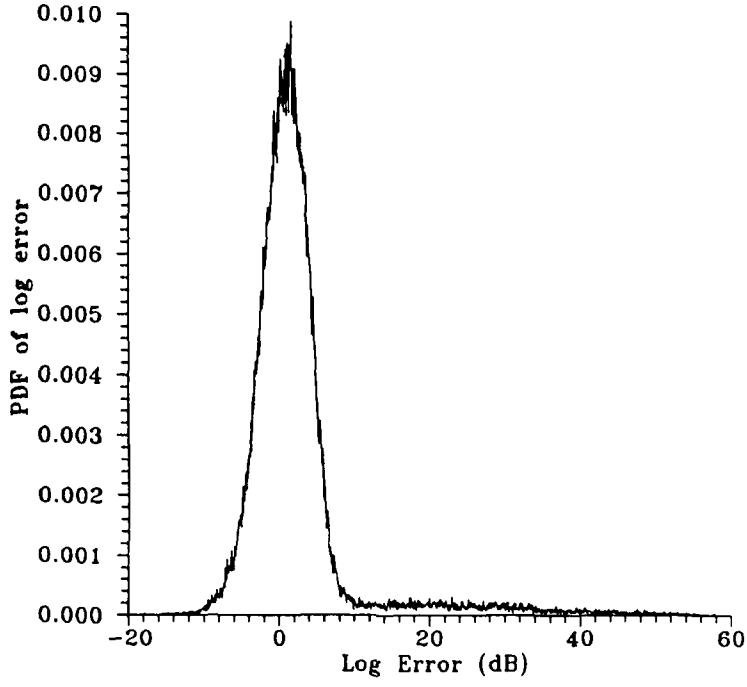

Figure 35 : Log-Error Histogram of GO-CFAR (0 x 4)

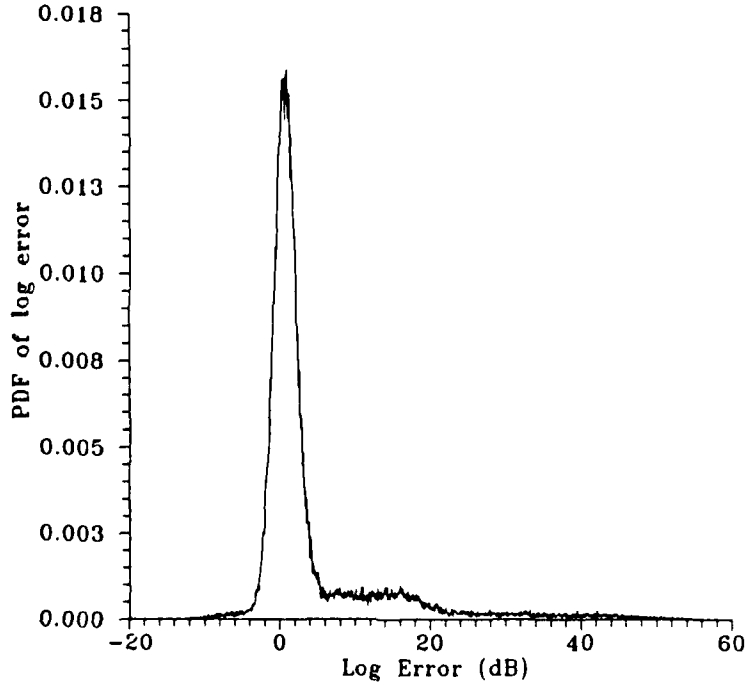

Figure 36 : Log-Error Histogram of GO-CFAR (4 x 4)

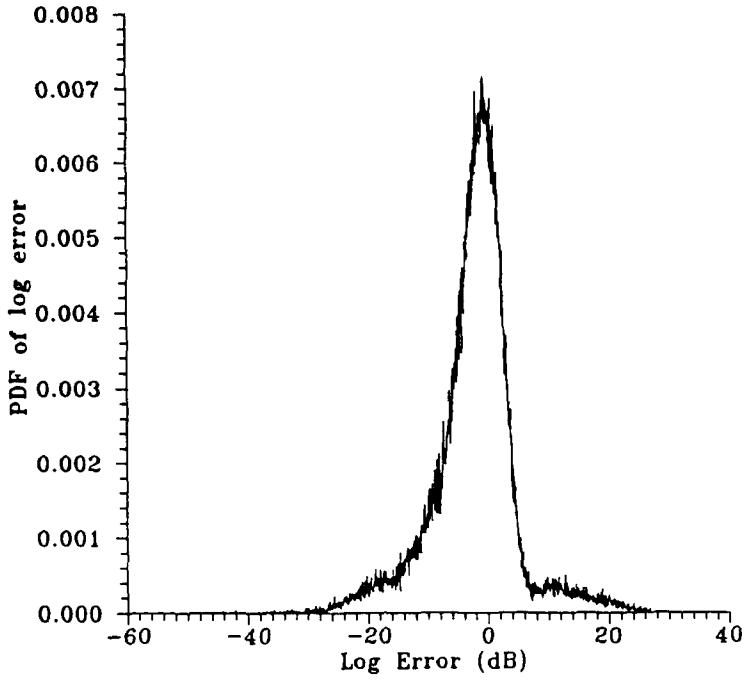

Figure 37 : Log-Error Histogram of SO-CFAR (4 x 0)

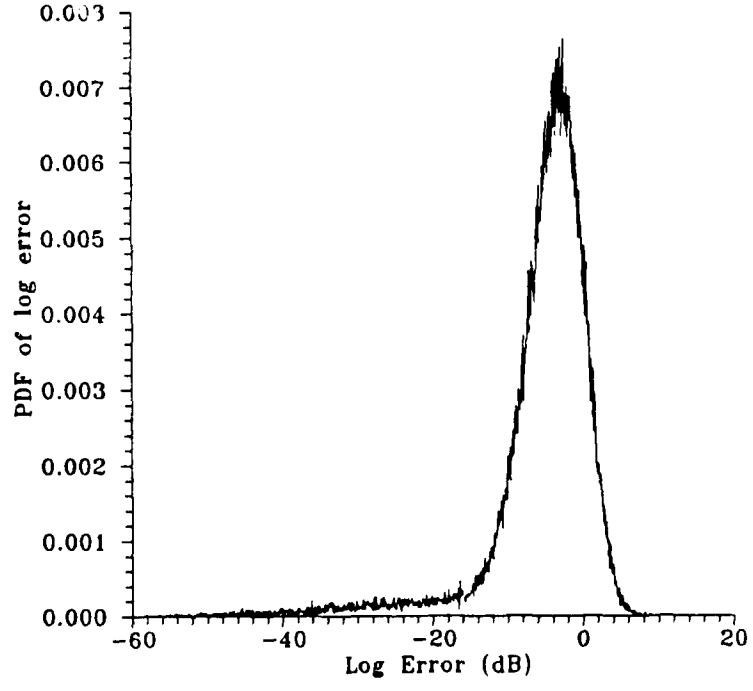

Figure 38 : Log-Error Histogram of SO-CFAR (0 x 4)

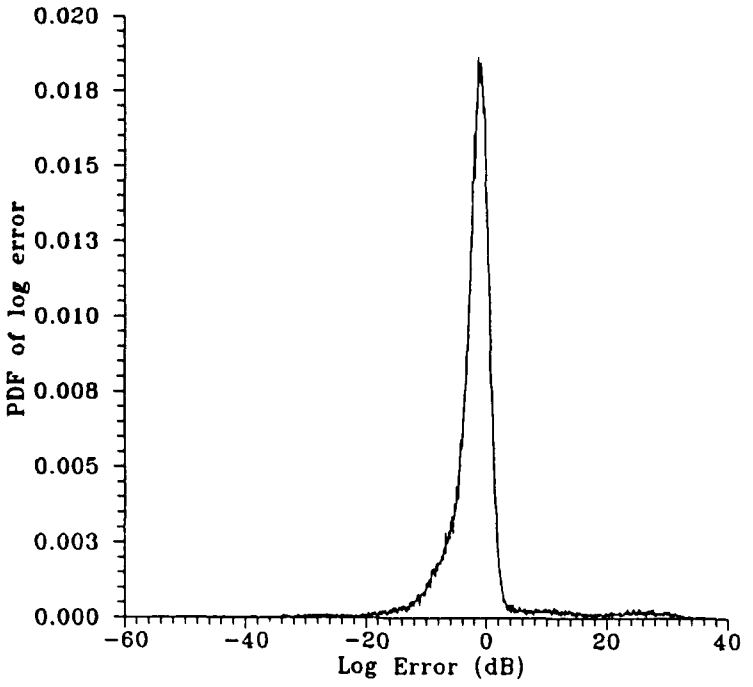

Figure 39 : Log-Error Histogram of SO-CFAR (4 x 4)

The threshold distribution functions of the three CFAR processors and a reference window size of 4x0 range-Doppler cells are plotted in Figure 40, for a false alarm rate of 10^{-3}. For the detection of a steady target with a probability of 0.5, the CFAR losses of the CA, GO and SO-CFAR processors are 20.2 dB, 20.5 dB, and 21.0 dB respectively. Increasing the probability of detection to 0.9 yields CFAR losses of 21.0 dB, 21.0 dB and 19.0 dB for the CA, GO and SO-CFAR processors, respectively. The reason why the performance of all three processors is so similar, in this case, is that with a 4x0 reference window, two subsets (one closer in range than the test cell, and one farther in range) are only formed if the test cell lies in the third range gate. If the test cell is in any other range gate, then only one subset is formed, and all three processors behave as a CA-CFAR processor. Figure 3 depicts the reference window scenario if the test cell lies in the fifth range gate.

In Figure 41 the threshold distribution functions are plotted for a reference window size of 0x4 cells and the severe underestimation problems of the SO-CFAR processor are vividly displayed. The CFAR losses of the CA, GO and SO processors are 6 dB, 7 dB and 37.5 dB for a detection probability of 0.5, and 6 dB, 7 dB and 30 dB for a detection probability of 0.9. The threshold distribution functions with a 4x4 reference window are displayed in Figure 42. This time the CFAR losses of the CA, GO, and SO-CFAR processors are 6.5 dB, 4.0 dB, and 33.0 dB for a 0.5 detection probability, and 15.5 dB, 15.5 dB, and 30.5 dB for a detection probability of 0.9.

Figures 43 to 45 illustrate the threshold distribution functions for the CA-CFAR, GO-CFAR and SO-CFAR processors, respectively, for reference window sizes of 2x0, 4x0, 6x0, 0x2, 0x4, and 0x8 and a false alarm rate of 10^{-3}. The smallest CFAR loss for the CA-CFAR processor occurred with the 0x8 window and had values of 4.2 dB for a 0.5 detection probability, and 5.0 dB for a 0.9 detection probability. Similarly the GO-CFAR processor had the best performance with the 0x8 reference window, resulting in CFAR losses of 4.5 dB and 6.6 dB for detection probabilities of 0.5 and 0.9, respectively. For both the CA and GO-CFAR processors, a one-dimensional reference window in the Doppler dimension produces CFAR losses approximately 17 dB smaller than the corresponding one-dimensional reference window in the range dimension. On the other hand, the SO-CFAR processor has an approximately 13 dB improvement in CFAR loss if the reference window is one-dimensional in range, rather than in Doppler. As explained earlier, this is because the smallest-of computation is only performed when the test cell is in the third range gate, if a range-only window is used. The underestimation problems of the SO-CFAR processor can only affect one-fifth of the total number of cells. Consequently, it is not unexpected that the SO-CFAR algorithm should perform better if the reference window is one-dimensional in range for the 5 x 128 maps studied in this report. The SO-CFAR 6x0 reference window incurred CFAR losses of 21 dB for a 0.5 detection probability, and 19 dB for a 0.9 detection probability.

In Figures 46 and 47 the threshold distribution functions of the CA and GO-CFAR algorithms are plotted for a false alarm rate of 10^{-6}, using the same reference windows as in the cases of Figures 43 and 44. Again, the 0x8 reference window results in the smallest CFAR loss. This loss is 8.5 dB and 9.5 dB for the CA and GO algorithms, with a steady target detection probability of 0.5. A probability of detection of 0.9 results in CFAR losses of 9.2 dB and 11.2 dB for the CA and GO-CFAR processors, respectively. As with the cases in which the false alarm rate was 10^{-3}, averaging with reference cells only in the range dimension does not work well.

The threshold distribution functions of the CA, GO, and SO-CFAR processors for a false alarm rate of 10^{-3}, and reference window sizes of 2x2, 4x4, 0x16, 0x40, and 2x16 are illustrated in Figures 48 to 50, respectively. Note that if none of the reference cells are 'cut-off' by the map's edge, then a 2x2 reference window has the same number of reference cells as a 0x16 window, and a 4x4 reference window has the same number of cells as a 0x40 window. The smallest CFAR losses of 3.4 dB, and 5.7 dB, for detection probabilities of 0.5 and 0.9, respectively, with the CA-CFAR processor were obtained using a 0x16 reference window. The GO-CFAR processor achieved CFAR losses of 2.8 dB using a 2x16 window at a 0.5 detection probability, and 7.5 dB using a 0x16 window at a 0.9 detection probability. CFAR losses of 32.5 dB (detection probability 0.5) with a 4x4 window, and 22.0 dB (detection probability 0.9) with a 0x40 window were obtained with the SO-CFAR processor.

In Figures 51 and 52 the threshold distributions of the CA and GO-CFAR processors are plotted using the reference windows listed above and a false alarm rate of 10^{-6}. In these cases, both processors achieved the smallest CFAR losses with a 0x16 reference window. The losses for a 0.5 detection probability were 6.5 dB for CA-CFAR, and 6.9 dB for GO-CFAR. A 0.9

probability of detection yielded CFAR losses of 8.8 dB for CA-CFAR and 10.8 dB for GO-CFAR.

Finally, the threshold distribution functions of the CA and GO-CFAR processors are compared in Figures 53 and 54 for reference windows of 2x2, 4x4, and 6x6 range-Doppler cells, at false alarm rates of 10^{-3}, and 10^{-6}, respectively. At $P_{fa} = 10^{-3}$, the smallest CFAR loss of 3.8 dB, for a 0.5 probability of detection was obtained with the GO-CFAR 6x6 processor. The GO-CFAR 2x2 processor had a CFAR loss of 12 dB at a 0.9 detection probability. When the false alarm rate was decreased to 10^{-6}, the GO-CFAR 6x6 processor had a CFAR loss of 10.9 dB at a probability of detection of 0.5, and the CA-CFAR 2x2 processor had a CFAR loss of 19 dB at a probability of detection of 0.9.

All of the threshold distribution plots presented illustrate the wide variability in performance which can be achieved by using different reference window sizes. In general, one dimensional Doppler reference windows worked the best for CA-CFAR and GO-CFAR, although two-dimensional windows also worked well for GO-CFAR. Increasing the size of the reference window usually improved performance, however, making the window too large can degrade the performance, as seen in the curves for the 0x40 reference window. If the window becomes too large, then part of the clutter peak will always lie within the reference window, resulting in threshold values which are larger than they need be.

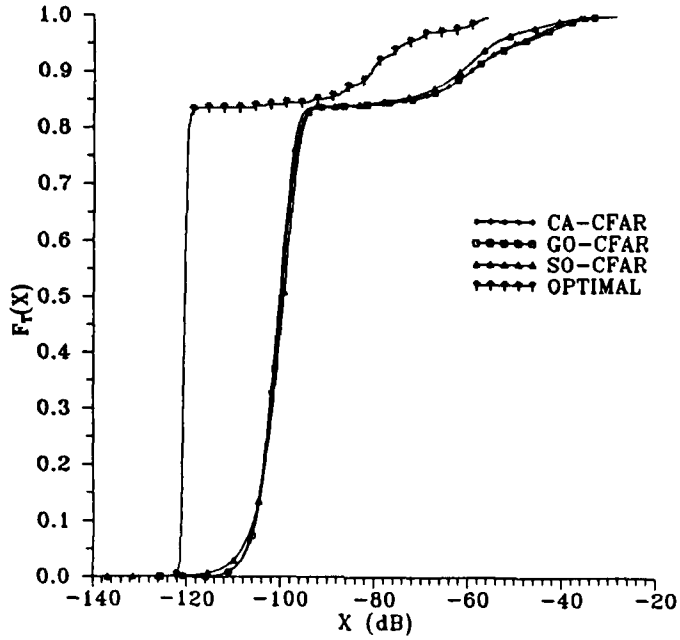

Figure 40 : Threshold Distribution Functions of a 4 x 0 Reference Window and $P_{fa} = 10^{-3}$.

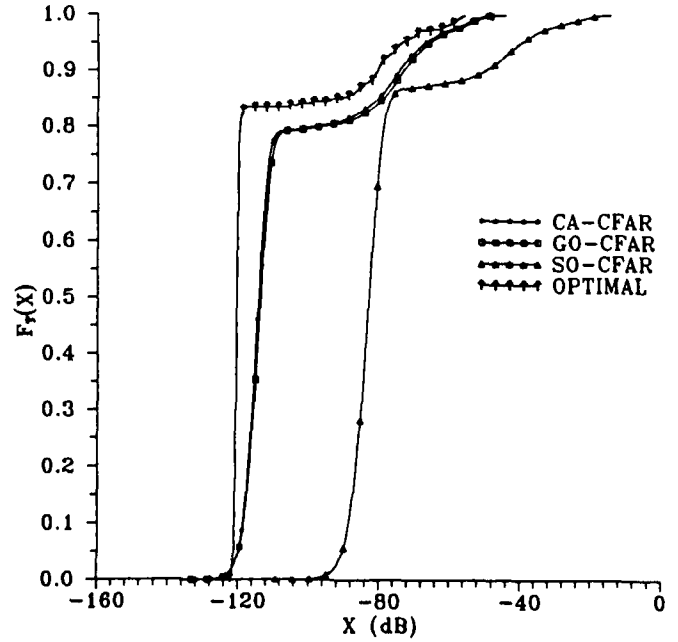

Figure 41 : Threshold Distribution Functions of a 0 x 4 Reference Window and $P_{fa} = 10^{-3}$.

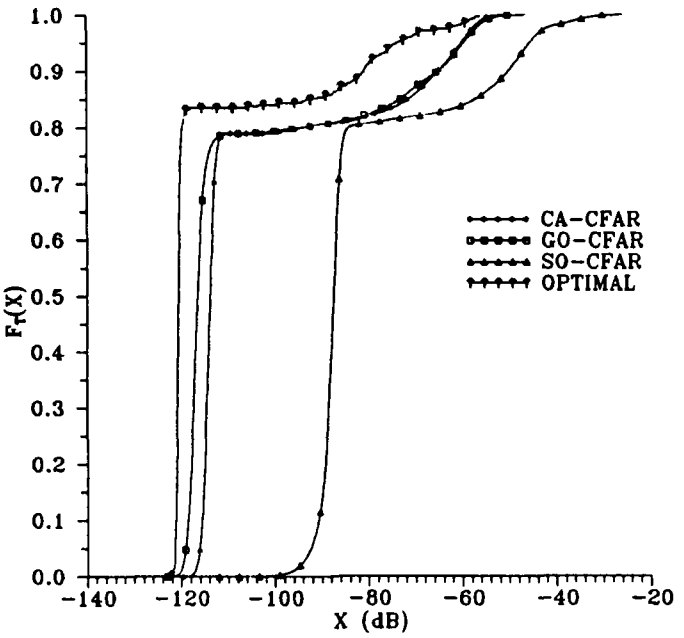

Figure 42 : Threshold Distribution Functions of a 4 x 4 Reference Window and $P_{fa} = 10^{-3}$.

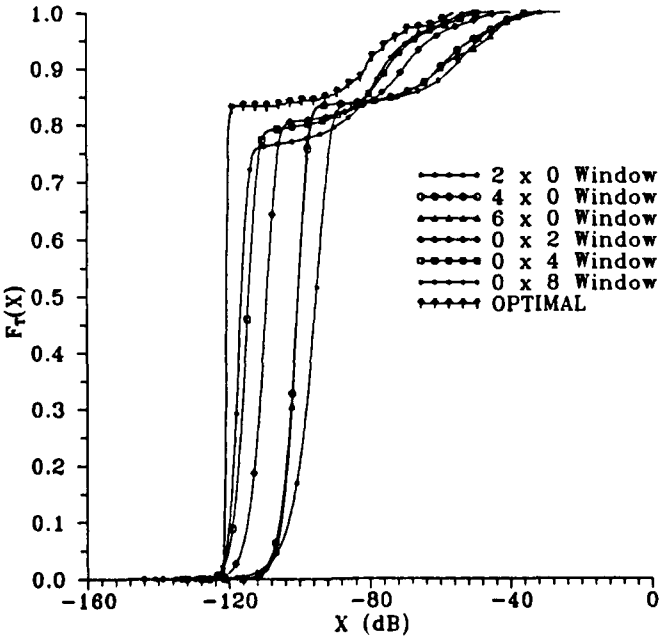

Figure 43 : Threshold Distribution Functions of CA-CFAR and $P_{fa} = 10^{-3}$.

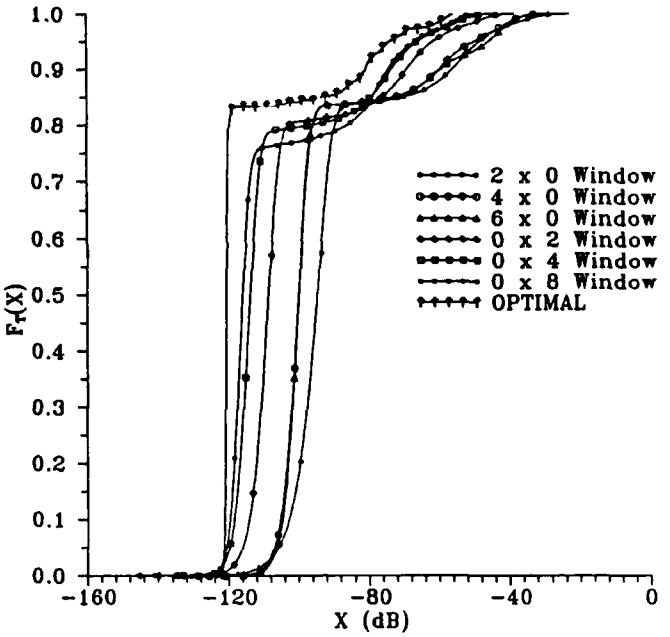

Figure 44 : Threshold Distribution Functions of GO-CFAR and $P_{fa} = 10^{-3}$.

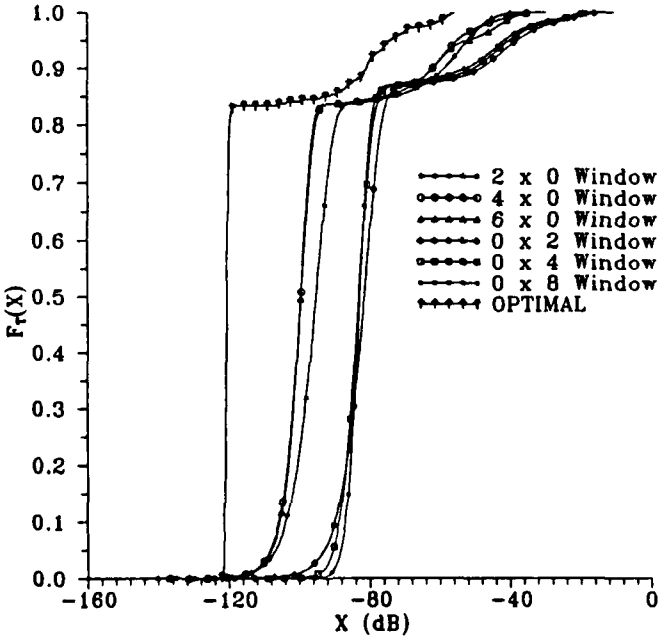

Figure 45 : Threshold Distribution Functions of SO-CFAR and $P_{fa} = 10^{-3}$.

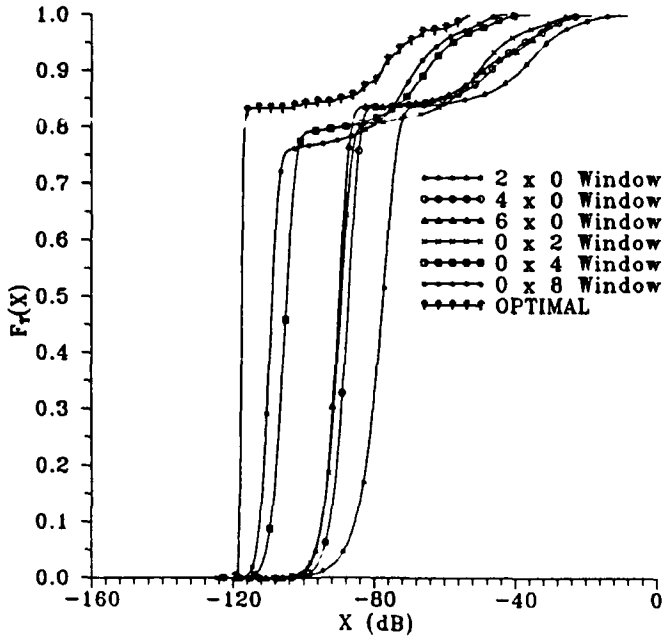

Figure 46 : Threshold Distribution Functions of CA-CFAR for $P_{fa} = 10^{-6}$.

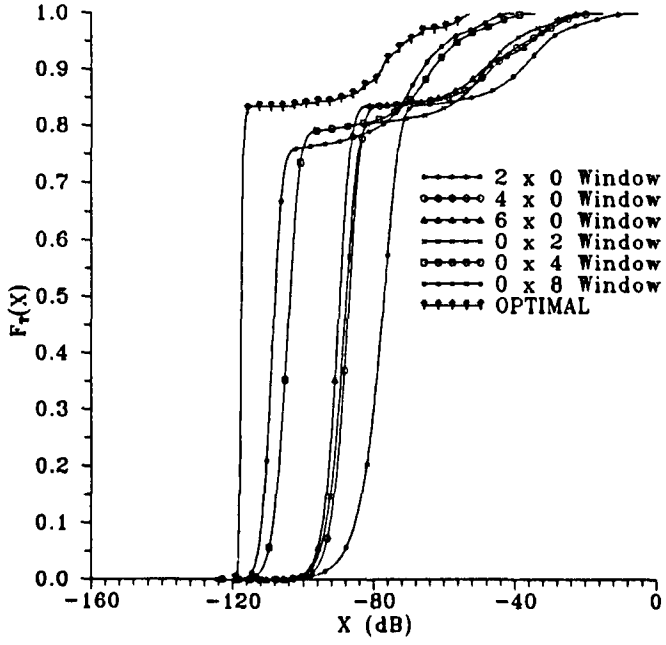

Figure 47 : Threshold Distribution Functions of GO-CFAR and $P_{fa} = 10^{-6}$.

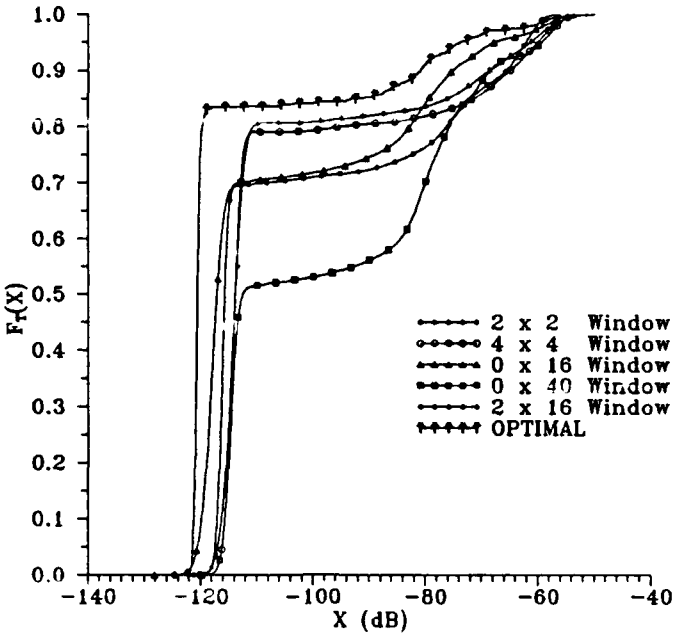

Figure 48 : Threshold Distribution Functions for CA-CFAR and $P_{fa} = 10^{-3}$.

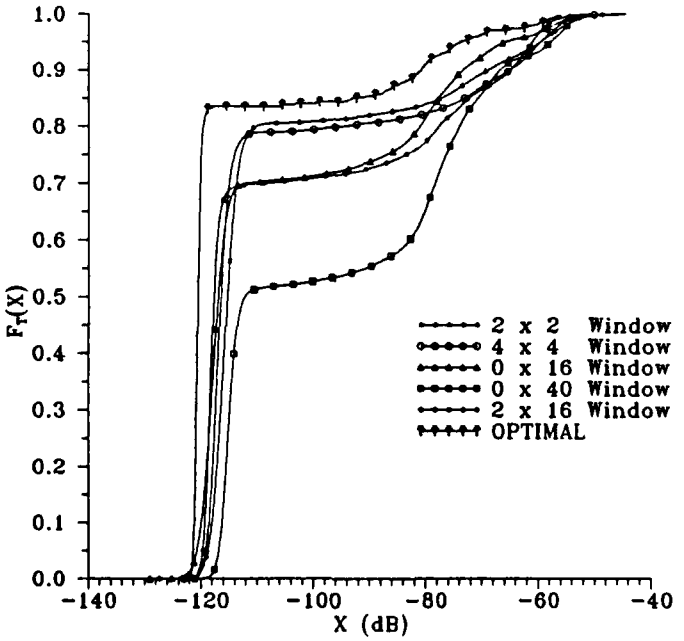

Figure 49 : Threshold Distribution Functions for GO-CFAR for $P_{fa} = 10^{-3}$.

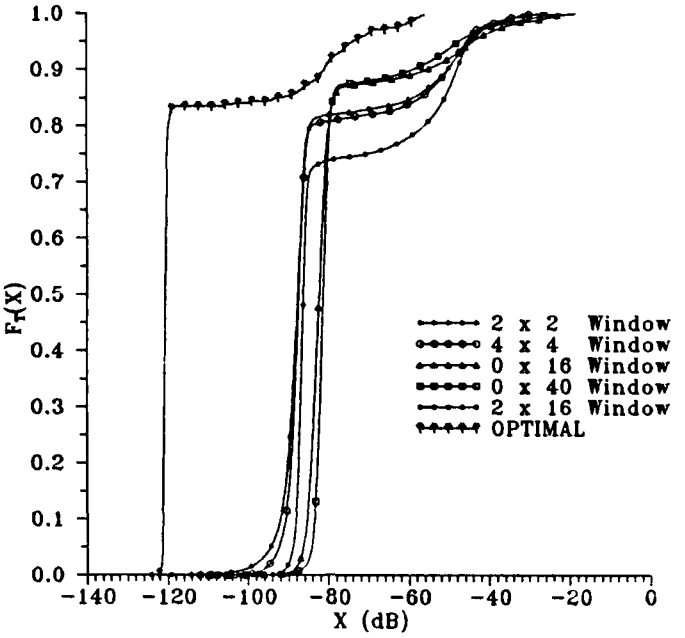

Figure 50 : Threshold Distribution Functions for SO-CFAR and $P_{fa} = 10^{-3}$.

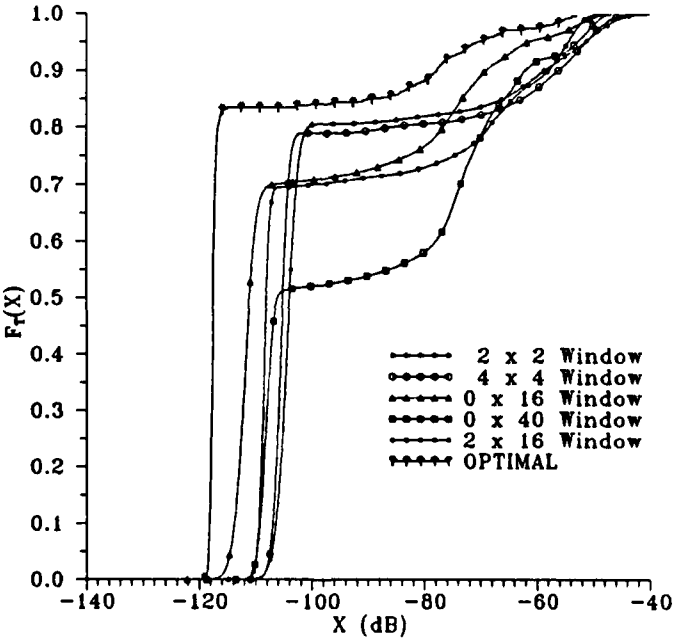

Figure 51 : Threshold Distribution Functions for CA-CFAR and $P_{fa} = 10^{-6}$.

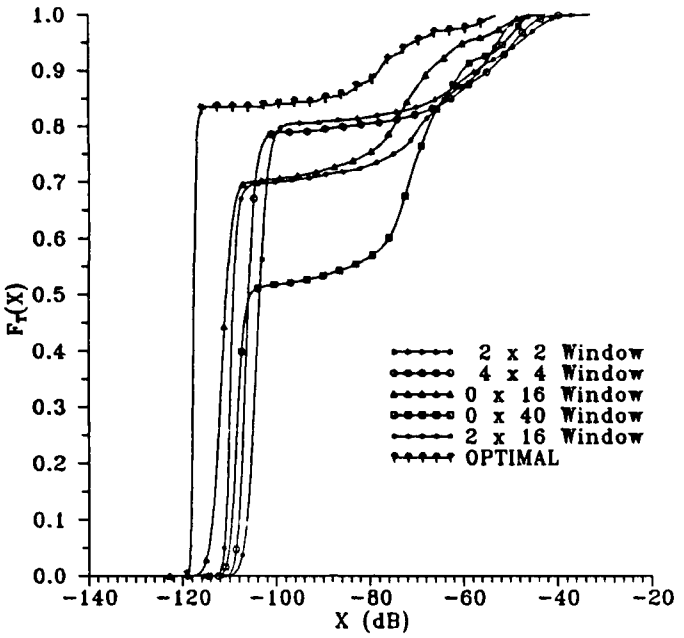

Figure 52 : Threshold Distribution Functions for GO-CFAR and $P_{fa} = 10^{-6}$.

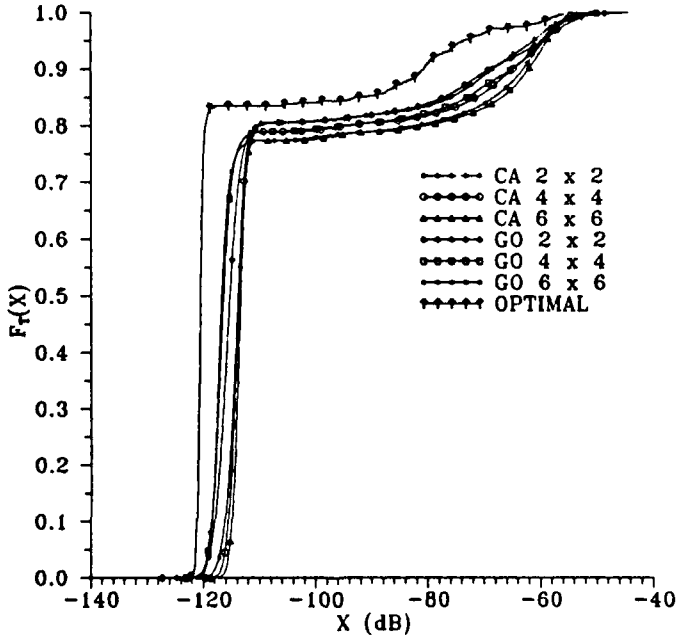

Figure 53 : Threshold Distribution Functions of CA-CFAR and GO-CFAR for $P_{fa} = 10^{-3}$.

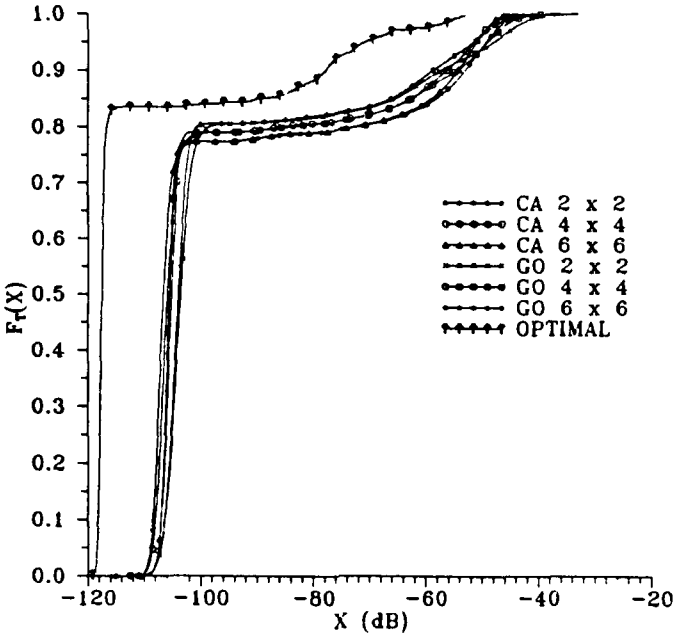

Figure 54 : Threshold Distribution Functions of CA-CFAR and GO-CFAR for $P_{fa} = 10^{-6}$.

8.0 CONCLUSIONS AND RECOMMENDATIONS FOR FURTHER RESEARCH

In this report a preliminary investigation of CFAR techniques for airborne pulse-Doppler radars was performed. A method for comparing different CFAR processors, by comparing their threshold distribution functions, was implemented and tested. Three different CFAR processors (cell-averaging, greatest-of, and smallest-of) were tested on interference environments of thermal noise, and thermal noise plus clutter. The importance of generating enough snapshots of data to obtain consistent threshold estimates was highlighted.

It was found that in general, the smallest-of CFAR processor performed much worse than either the cell-averaging, or the greatest-of processors, because it tends to underestimate the interference power. The SO-CFAR processor had its best performance when the reference window was one-dimensional in the range dimension, because, as was described, its underestimation problems could only affect one-fifth of the total number of cells. Even then it was still worse than the CA or GO-CFAR processors. Generally, the best results for the CA-CFAR processor were obtained with one-dimensional Doppler windows, while two-dimensional windows worked best for GO-CFAR.

Both the CA and GO-CFAR processors worked very well in the thermal noise environment (CFAR losses < 0.6 dB). However, the severe peak in the clutter environment caused serious degradations in their performance. To achieve a particular false alarm rate, the CFAR algorithms raise the threshold considerably, to accommodate the large clutter peak. In fact all of the false alarms that occurred in the ensemble of maps, were from the clutter peak region.

In the noise dominated region, outside of the clutter peak, the very large threshold is much higher than it need be. As a result, the system is less sensitive to targets which may appear in this region. Further work must be done to examine this situation. Perhaps some other CFAR techniques such as Ordered Statistic (OS), or the gradient method would improve the results. Perhaps the clutter peak could be ignored completely, essentially reducing the problem to the noise-only environment, or alternatively some sort of adaptive window scheme could be developed. Since the location of the clutter peak region is known a priori, it should be possible to design a processor which excludes the clutter peak from the reference window if the test cell lies in the noise-only region, or exclude the noise region from the reference window if the test cell lies in the clutter peak region.

The simulations involving clutter in this report were performed for a specific set of radar parameters and geometry. Further work should investigate the effects of different geometries (radar altitude, look angles etc.) on the threshold multiplier and threshold distribution functions. If it is found that the threshold values are highly dependent upon the geometry of the radar and clutter patches, then an adaptive scheme to continually determine the appropriate values may be required.

REFERENCES

1. **Finn H.M., and Johnson R.S. (1968)**
   Adaptive Detection Mode with Threshold Control as a Function of Spatially Sampled Clutter-Level Estimates.
   RCA Review, Vol. 29, No. 3, September 1968, pp. 414-464.

2. **Minkler G., and Minkler J. (1990)**
   CFAR : The Principles of Automatic Radar Detection in Clutter.
   Magellan Book Company, Baltimore, MD, 1990.

3. **Weber P., Haykin S., and Gray R. (1987)**
   Airborne Pulse-Doppler Radar: False-Alarm Control.
   IEE Proceedings, Vol. 134, Pt. F, No. 2, April 1987, pp. 127-134.

4. **Weiss M (1982)**
   Analysis of Some Modified Cell-Averaging CFAR Processors in Multiple-Target Situations.
   IEEE Transactions on Aerospace and Electronic Systems, Vol. AES-18, No. 2, March 1982, pp. 242-248.

5. **Hansen V.G. (1973)**
   Constant False Alarm Rate Processing in Search Radars.
   IEE Conference Publication No. 105, "Radar-Present and Future", London, October 23-25 1973, pp. 325-332.

6. **Nitzberg R. (1973)**
   Constant-False-Alarm-Rate Processors for Locally Nonstationary Clutter.
   IEEE Transactions on Aerospace and Electronic Systems, Vol. AES-9, No. 3, May 1973, pp. 399-405.

7. **Rohling H. (1983)**
   Radar CFAR Thresholding in Clutter and Multiple Target Simulations.
   IEEE Transactions on Aerospace and Electronic Systems, Vol. AES-19, No. 4, July 1983, pp. 608-621.

8. **Schleher D. C. (1980)**
   Automatic Detection and Radar Data Processing.
   Artech House Inc., Dedham, MA, 1980.

9. **Farina A., and Studer F.A. (1986)**
   A Review of CFAR Detection Techniques in Radar Systems.
   Microwave Journal, September 1986, pp. 115-128.

10. **Elias-fuste A.R., de Mercado M.G.G., and de los Reyes Davo E. (1990)**
Analysis of Some Modified Ordered Statistic CFAR: OSGO and OSSO CFAR.
IEEE Transactions on Aerospace and Electronic Systems, Vol. AES-26, No. 1, January 1990, pp. 197-202.

11. **Faubert D. (1989)**
A Theoretical Model for Airborne Radars.
Defence Research Establishment Ottawa Report No. 1017, PCN 21LA12, November 1989.

12. **Vineberg K.A., and Saper R. (1989)**
Updates to the DREO Airborne Radar Simulator.
Atlantis Scientific Systems Group Inc. Report No. 167, June 1989.

13. **Gibb M., Lightstone L., and Saper R. (1988)**
Pulse Doppler Radar Simulation Study: Final Technical Report.
Atlantis Scientific Systems Group Inc. Report No. TR-20, October 1988.

14. **Lightstone L. (1988)**
Behaviour of the SIR for Space-Based DPCA Radar Under Various Spatial Clutter Distributions.
Atlantis Scientific Systems Group Inc. Report No. TR-11, February 1988.

15. **Lightstone L. (1987)**
A Model of a Displaced Phase Centre Antenna System for Space-Based Radar with Generalized Orbital Parameters and Earth Rotation.
Atlantis Scientific Systems Group Inc., Call Up Number W7714-06-5121, July 1987.

16. **Meyer P.L. (1970)**
Introductory Probability and Statistical Applications (Second Edition).
Addison-Wesley Publishing Company, Reading MA, 1970.

17. **Weber P., and Haykin S. (1985)**
Airborne Pulse-Doppler Radar: False Alarm Control.
Communications Research Laboratory Report CRL-147, McMaster University, Hamilton, Ont., September 1985.

UNCLASSIFIED

SECURITY CLASSIFICATION OF FORM
(highest classification of Title, Abstract, Keywords)

DOCUMENT CONTROL DATA

(Security classification of title, body of abstract and indexing annotation must be entered when the overall document is classified)

1. ORIGINATOR (the name and address of the organization preparing the document. Organizations for whom the document was prepared, e.g. Establishment sponsoring a contractor's report, or tasking agency, are entered in section 8.)

Defence Research Establishment Ottawa
3701 Carling Avenue
Ottawa, Ontario, Canada K1A 0Z4

2. SECURITY CLASSIFICATION (overall security classification of the document. including special warning terms if applicable)

UNCLASSIFIED

3. TITLE (the complete document title as indicated on the title page. Its classification should be indicated by the appropriate abbreviation (S,C,R or U) in parentheses after the title.)

An Investigation of CFAR Techniques for Airborne Radars (U)

4. AUTHORS (Last name, first name, middle initial)

VRCKOVNIK Gary E., FAUBERT Denis

5. DATE OF PUBLICATION (month and year of publication of document)

DECEMBER 1990

6a. NO. OF PAGES (total containing information. Include Annexes, Appendices, etc.)

52

6b. NO. OF REFS (total cited in document)

17

7. DESCRIPTIVE NOTES (the category of the document, e.g. technical report, technical note or memorandum. If appropriate, enter the type of report, e.g. interim, progress, summary, annual or final. Give the inclusive dates when a specific reporting period is covered.)

DREO Technical Report

8. SPONSORING ACTIVITY (the name of the department project office or laboratory sponsoring the research and development. Include the address.)

Defence Research Establishment Ottawa
3701 Carling Avenue
Ottawa, Ontario, Canada K1A 0Z4

9a. PROJECT OR GRANT NO. (if appropriate, the applicable research and development project or grant number under which the document was written. Please specify whether project or grant)

021LA

9b. CONTRACT NO. (if appropriate, the applicable number under which the document was written)

10a. ORIGINATOR'S DOCUMENT NUMBER (the official document number by which the document is identified by the originating activity. This number must be unique to this document.)

DREO REPORT 1056

10b. OTHER DOCUMENT NOS. (Any other numbers which may be assigned this document either by the originator or by the sponsor)

11. DOCUMENT AVAILABILITY (any limitations on further dissemination of the document, other than those imposed by security classification)

(X) Unlimited distribution
( ) Distribution limited to defence departments and defence contractors; further distribution only as approved
( ) Distribution limited to defence departments and Canadian defence contractors; further distribution only as approved
( ) Distribution limited to government departments and agencies; further distribution only as approved
( ) Distribution limited to defence departments; further distribution only as approved
( ) Other (please specify):

12. DOCUMENT ANNOUNCEMENT (any limitation to the bibliographic announcement of this document. This will normally correspond to the Document Availability (11). However, where further distribution (beyond the audience specified in 11) is possible, a wider announcement audience may be selected.)

UNCLASSIFIED

SECURITY CLASSIFICATION OF FORM

DCD03 2/06/87

UNCLASSIFIED

SECURITY CLASSIFICATION OF FORM

13. ABSTRACT (a brief and factual summary of the document. It may also appear elsewhere in the body of the document itself. It is highly desirable that the abstract of classified documents be unclassified. Each paragraph of the abstract shall begin with an indication of the security classification of the information in the paragraph (unless the document itself is unclassified) represented as (S), (C), (R), or (U). It is not necessary to include here abstracts in both offical languages unless the text is bilingual).

In this report, techniques for performing constant false alarm rate (CFAR) processing, with airborne pulse-Doppler radars are described. Cell-averaging, greatest-of, and smallest-of CFAR processors are implemented on interference environments of thermal noise, and thermal noise plus clutter. For the particular radar conditions considered, a 60 dB clutter peak appears across all of the range gates. While these three processors were successful in the thermal noise environment, they suffered large CFAR losses in the presence of the clutter peak. The smallest-of CFAR algorithm performed much worse than the other two, due to its tendency to underestimate the interference powers. Although enlarging the reference window improves the performance of all the processors, it is clear that for the complicated clutter situation examined, more sophisticated CFAR techniques are required.

14. KEYWORDS, DESCRIPTORS or IDENTIFIERS (technically meaningful terms or short phrases that characterize a document and could be helpful in cataloguing the document. They should be selected so that no security classification is required. Identifiers, such as equipment model designation, trade name, military project code name, geographic location may also be included. If possible keywords should be selected from a published thesaurus. e.g. Thesaurus of Engineering and Scientific Terms (TEST) and that thesaurus-identified. If it is not possible to select indexing terms which are Unclassified, the classification of each should be indicated as with the title.)

Constant false alarm rate processors, CFAR, Cell-averaging, Greatest-of, Smallest-of, airborne pulse-Doppler radar, clutter

UNCLASSIFIED

SECURITY CLASSIFICATION OF FORM